© 2015. Published by The Company of Biologists Ltd | Journal of Cell Science (2015) 128, 1386–1399 doi:10.1242/jcs.163857

RESEARCH ARTICLE

The Rho-specific GAP protein DLC3 coordinates endocytic membrane trafficking

Anja C. Braun, Janina Hendrick, Stephan A. Eisler, Simone Schmid, Angelika Hausser and Monilola A. Olayioye*

ABSTRACT

Membrane trafficking is known to be coordinated by small GTPases, but the identity of their regulators, the guanine nucleotide exchange factors (GEFs) and GTPase-activating proteins (GAPs) that ensure balanced GTPase activation at different subcellular sites is largely elusive. Here, we show in living cells that deleted in liver cancer 3 (DLC3, also known as STARD8) is a functional Rho-specific GAP protein, the loss of which enhances perinuclear RhoA activity. DLC3 is recruited to Rab8-positive membrane tubules and is required for the integrity of the Rab8 and Golgi compartments. Depletion of DLC3 impairs the transport of internalized transferrin to the endocytic recycling compartment (ERC), which is restored by the simultaneous downregulation of RhoA and RhoB. We further demonstrate that DLC3 loss interferes with epidermal growth factor receptor (EGFR) degradation associated with prolonged receptor signaling. Taken together, these findings identify DLC3 as a novel component of the endocytic trafficking machinery, wherein it maintains organelle integrity and regulates membrane transport through the control of Rho activity.

KEY WORDS: Rho GTPase-activating protein, Endocytosis, Rab8, Tumor suppressor, EGFR signaling

INTRODUCTION

Small GTPases of the Rho family are key regulators of the actin and microtubule cytoskeleton, thereby controlling different steps of cell migration, adhesion and polarity, cell cycle progression and differentiation (Jaffe and Hall, 2005). Owing to their fundamental role in actin-myosin dynamics, Rho GTPases are also crucially involved in intracellular trafficking, with Cdc42, Rho and Rac studied most extensively (Chi et al., 2011; Qualmann and Mellor, 2003; Symons and Rusk, 2003). Apart from its function at the plasma membrane in the regulation of endo- and exocytosis, active Cdc42 has been shown to localize to the Golgi complex (Nalbant et al., 2004), where it regulates polarized post-Golgi traffic and Golgi-to-ER transport (Harris and Tepass, 2010; Luna et al., 2002; Müsch et al., 2001). In the case of the Rho subfamily members, RhoA has mainly been associated with membrane trafficking events at the plasma membrane. For example, activated RhoA was reported to inhibit clathrin-dependent internalization of the transferrin receptor (Lamaze et al., 1996). Associated with the distinct localization of RhoB to endocytic vesicles (Adamson et al., 1992; Robertson et al., 1995), activated RhoB induces actin assembly on endosomes, causing reduced motility and thereby affecting endosomal vesicle dynamics (Fernandez-Borja et al., 2005).

Small GTPases function as molecular switches cycling between an active GTP-bound state and an inactive GDP-bound state. The activity of small GTPases is controlled by GEFs, which promote the exchange of bound GDP for GTP, leading to GTPase activation, and GAPs, which accelerate the low intrinsic GTPase activity and thereby lead to GTPase inactivation (Bos et al., 2007; Vigil et al., 2010). Although GAPs and GEFs are crucial for the control of Rho GTPases, within vesicle trafficking only a few regulators are known so far. Focusing on Rho, the GAP protein GMIP and GEF-H1 (also known as ARHGEF2) have been shown to be important for local RhoA regulation during exocytosis (Johnson et al., 2012; Pathak et al., 2012). In the context of receptor-mediated endocytosis, p50RhoGAP (also known as ARHGAP1) has been proposed to regulate crosstalk between Rab and Rho GTPases (Sirokmány et al., 2006). Overexpressed p50RhoGAP has been found to colocalize with Rab5- and Rab11-positive endosomal membranes and to inhibit transferrin uptake (Sirokmány et al., 2006).

The ‘deleted in liver cancer 1, 2 and 3 proteins’ (DLC1, DLC2 and DCL3; hereafter referred to as STARD12, STARD13 and STARD8, respectively) are a structurally conserved subfamily of GAP proteins that further contain a sterile α motif (SAM) and a steroidogenic acute regulatory protein-related lipid transfer (START) domain (Durkin et al., 2007a). Expression of the focal-adhesion-associated DLC1 protein is frequently lost in various types of human cancers and a tumor-suppressive function associated with its RhoGAP activity has been established *in vivo* (Xue et al., 2008). DLC3 has also been observed to be downregulated in several cancer cell lines and primary tumors (Durkin et al., 2007b), but its cellular function is still poorly characterized, and GAP activity for RhoA has only been demonstrated *in vitro* (Holeiter et al., 2012; Kawai et al., 2007). Our group previously reported a role for DLC3 in adherens junction stability and cell differentiation associated with its localization at cell–cell contacts in breast epithelial cells (Holeiter et al., 2012). Here, we show for the first time in living cells that DLC3 possesses Rho-inhibitory activity, and we provide insight into the subcellular aspects of RhoA regulation by DLC3. Importantly, our study identifies DLC3 as a novel component of the endocytic recycling pathway, wherein it regulates Rho activity to determine membrane trafficking routes.

RESULTS

DLC3 colocalizes with Rab8 and affects ERC and Golgi morphology in a GAP-dependent manner

To obtain a better understanding of the cellular functions of DLC3, we first investigated the localization of DLC3 in HeLa cells. For these studies, we transiently transfected cells with

Institute of Cell Biology and Immunology, University of Stuttgart, Allmandring 31, 70569 Stuttgart, Germany.

*Author for correspondence (monilola.olayioye@izi.uni-stuttgart.de)

Received 26 September 2014; Accepted 2 February 2015

Journal of Cell Science

Journal of Cell Science (2015) 128, 1386–1399 doi:10.1242/jcs.163857

fluorescently tagged DLC3 variants, corresponding to the full-length DLC3α isoform (Fig. 1), because neither commercially available nor our custom-made DLC3-specific antibodies were suited for the detection of the endogenous protein by immunofluorescence. The ectopically expressed DLC3 wild-type (WT) protein caused severe morphological changes and a complete loss of actin stress fibers (supplementary material Fig. S1A,B), most likely associated with its GAP function. Interestingly, in cells expressing very low DLC3 levels, the Golgi complex appeared to be more compact (Fig. 1). However, although DLC3-WT was concentrated in the perinuclear region, little colocalization with the cis- and medial-Golgi protein giantin (also known as GOLGB1) was observed (Fig. 1). We therefore analyzed the potential colocalization of DLC3 with the ERC, located in close vicinity to the Golgi complex. The small GTPase Rab11 is the best characterized component of the ERC, but has also been found at the TGN. Its main function is the regulation of the slow recycling of endocytosed cargo from the ERC to the plasma membrane (Grant and Donaldson, 2009; Stenmark, 2009). GFP-tagged Rab11 partially colocalized with DLC3-WT in the perinuclear region, where it accumulated in the presence of DLC3 (Fig. 1). Interestingly, DLC3-WT strongly colocalized with endogenous Rab8, a further constituent of the ERC involved in membrane recycling, with additional functions in cell migration, epithelial polarization, ciliogenesis and neuronal differentiation (Peränen, 2011). Furthermore, expression of DLC3-WT caused obvious compaction of the Rab8 compartment, which, in contrast to untransfected cells, displayed no tubular structures (Fig. 1).

To investigate the contribution of the GAP activity to DLC3 localization and function, we expressed a mutant containing an inactivating amino acid substitution in the GAP domain (K725E) (Holeiter et al., 2012). Using the fluorescence resonance energy transfer (FRET)-based RhoA biosensor pTriEx-RhoA (Pertz et al., 2006), we measured RhoA activity in cells expressing either DLC3-WT or -K725E. Expression of DLC3-WT caused a significant decrease in FRET efficiency, proving the inhibitory function of DLC3 towards RhoA (supplementary material Fig. S1C). In line with the inactivation of its GAP activity, DLC3-K725E expression had no impact on the FRET efficiency (supplementary material Fig. S1C). Consistent with this, ectopic expression of DLC3-K725E caused no obvious changes in stress fiber formation, and the cells maintained a spread morphology (supplementary material Fig. S1A,B), making the GAP-inactive mutant suited for more detailed localization studies of the protein. Based on the comparable RhoA activities and F-actin contents in control and DLC3-K725E-expressing cells, GAP-inactive DLC3 does not appear to act in a dominant-negative manner, at least with respect to Rho signaling.

Similar to DLC3-WT, only minimal overlap with the Golgi membranes was observed in cells expressing GAP-inactive DLC3 (Fig. 2A). Interestingly, in many cells, DLC3-K725E was observed on tubular structures, which emerged from the perinuclear region and reached to the cell periphery (Fig. 2A). These tubules displayed a remarkable colocalization with Rab8-positive tubules or were decorated by orderly aligned Rab8 puncta (Fig. 2A). The formation of Rab8 tubules is dependent on actin dynamics and the biogenesis of tubules can be induced by treatment with cytochalasin D (CytD) (Hattula et al., 2006). To show that DLC3 is associated with Rab8 tubules, we treated DLC3-K725E-expressing cells with CytD. Upon treatment, the number of cells exhibiting prominent Rab8 tubulation increased significantly (Fig. 2A). This was accompanied by the distribution of DLC3-K725E to a network of tubular membranes that extensively overlapped with Rab8 (Fig. 2A,B). Quantification revealed that ~60% of the total cellular Rab8 signal overlapped with that of DLC3-K725E (Fig. 2B).

To examine whether DLC3-K725E associates with other tubulovesicular carriers or whether this association is restricted to Rab8-positive structures, we co-expressed DLC3-K725E and Rab11. Here, CytD treatment did not cause obvious redistribution of Rab11, which was found in small vesicular structures near the plasma membrane and the perinuclear region, and Rab11 did not

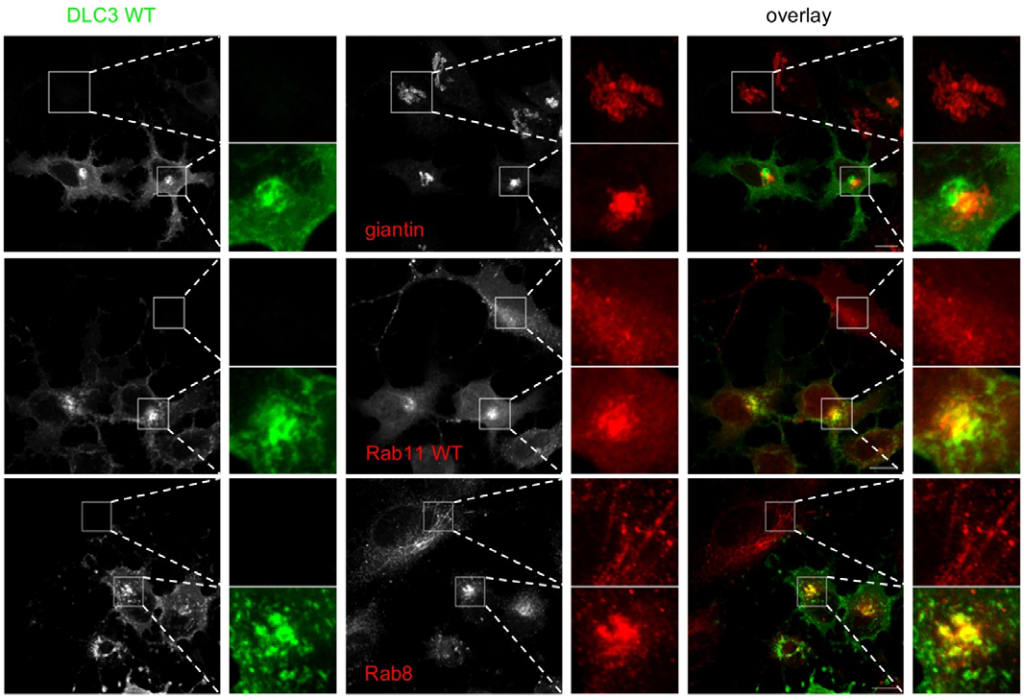

Fig. 1. Ectopically expressed wild-type DLC3 colocalizes with Rab8 and affects ERC and Golgi morphology. HeLa cells expressing GFP-tagged DLC3-WT (green) were stained for either giantin or Rab8 (red). In the case of Rab11, cells were co-transfected with vectors encoding mCherry–DLC3-WT (depicted in green) and GFP–Rab11-WT (depicted in red). Scale bars: 10 µm.

Journal of Cell Science (2015) 128, 1386–1399 doi:10.1242/jcs.163857

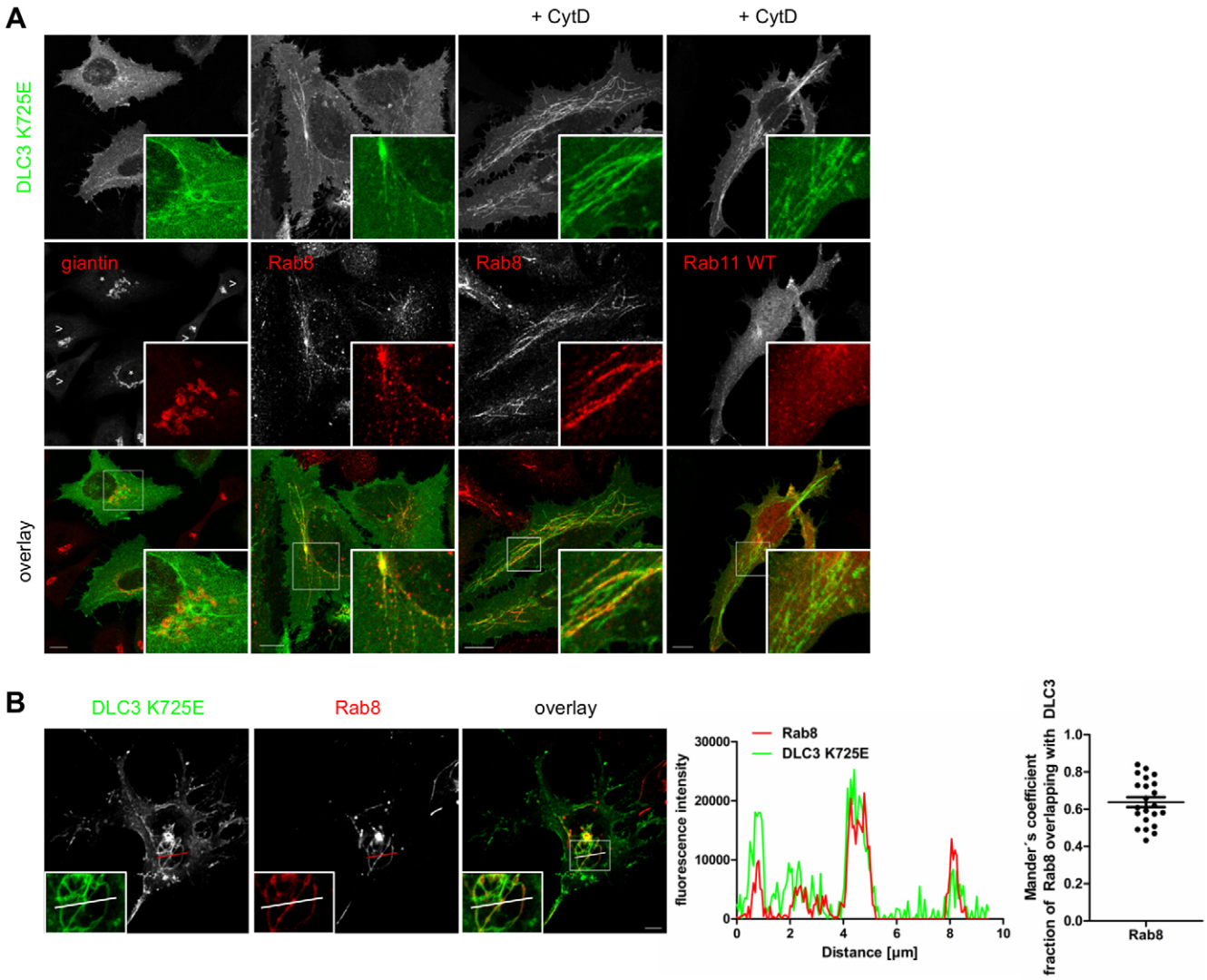

Fig. 2. Colocalization of GAP-inactive DLC3 with Rab8-positive tubules. (A) HeLa cells expressing GFP-tagged DLC3-K725E (green) were either stained for giantin or Rab8 (red). In the case of Rab11, cells were co-transfected with vectors encoding mCherry–DLC3-K725E (depicted in green) and GFP–Rab11-WT (depicted in red). Where indicated, cells were incubated with 0.1 µm CytD for 30 min (+ CytD). Scale bars: 10 µm. (B) Left panel, DLC3-K725E-expressing cells (green) were treated with CytD and stained for Rab8 (red). Scale bar: 5 µm. Middle panel, the fluorescence intensities of both signals along the white line are depicted. Right panel, quantification of the fraction of Rab8 overlapping with GFP–DLC3-K725E. Data show the mean±s.e.m. (N=20).

localize to DLC3-K725E-positive tubules before and after CytD treatment (Fig. 2A). Moreover, Rab6, which localizes to Golgi membranes (Goud et al., 1990; Liu and Storrie, 2012) and also associates with Rab8-positive post-Golgi carriers (Wakana et al., 2012), failed to colocalize with DLC3-K725E-positive tubules (supplementary material Fig. S1D). Although partial overlap with the trans-Golgi marker TGN46 (also known as TGOLN2) was detected at the center of emerging tubules, TGN46 was not found on DLC3-K725E-positive tubules (supplementary material Fig. S1D). Real-time imaging further revealed the presence of DLC3 on vesicles moving towards and away from the plasma membrane (data not shown), a subset of which were positive for endosomal RhoB (supplementary material Fig. S1D) (Adamson et al., 1992; Robertson et al., 1995). Taken together, these data suggest that the dynamic recruitment of ectopically expressed DLC3 to the Golgi–ERC interface occurs independently of its GAP activity, whereas the morphological and cytoskeletal changes associated with the inactivation of RhoA signaling require a functional GAP domain.

DLC3 is required for the integrity of the Rab8 and Golgi compartments

Owing to the localization of the ectopically expressed protein, DLC3 is a candidate GAP that, through Rho proteins, regulates the morphology and/or function of the Rab8-positive ERC. Indeed, overexpression of constitutively active RhoA-G14V induced vesiculation of the tubular Rab8 compartment (Fig. 3A). In addition, RhoA hyperactivation was shown to cause severe Golgi fragmentation (Zilberman et al., 2011) (Fig. 3A). Considering the partial colocalization of DLC3 with the trans-Golgi marker TGN46 (supplementary material Fig. S1D) and the fact that spatial analysis of RhoA activity revealed an inactive Golgi-localized pool of RhoA (Pertz et al., 2006), DLC3 might be involved in the negative regulation of Rho signaling at this subcellular site as well.

To assess the effects of DLC3 depletion on organelle morphology, we transiently transfected HeLa cells with DLC3-specific SMARTpool small interfering (si)RNAs and confirmed efficient downregulation of endogenous DLC3 expression by

Journal of Cell Science (2015) 128, 1386–1399 doi:10.1242/jcs.163857

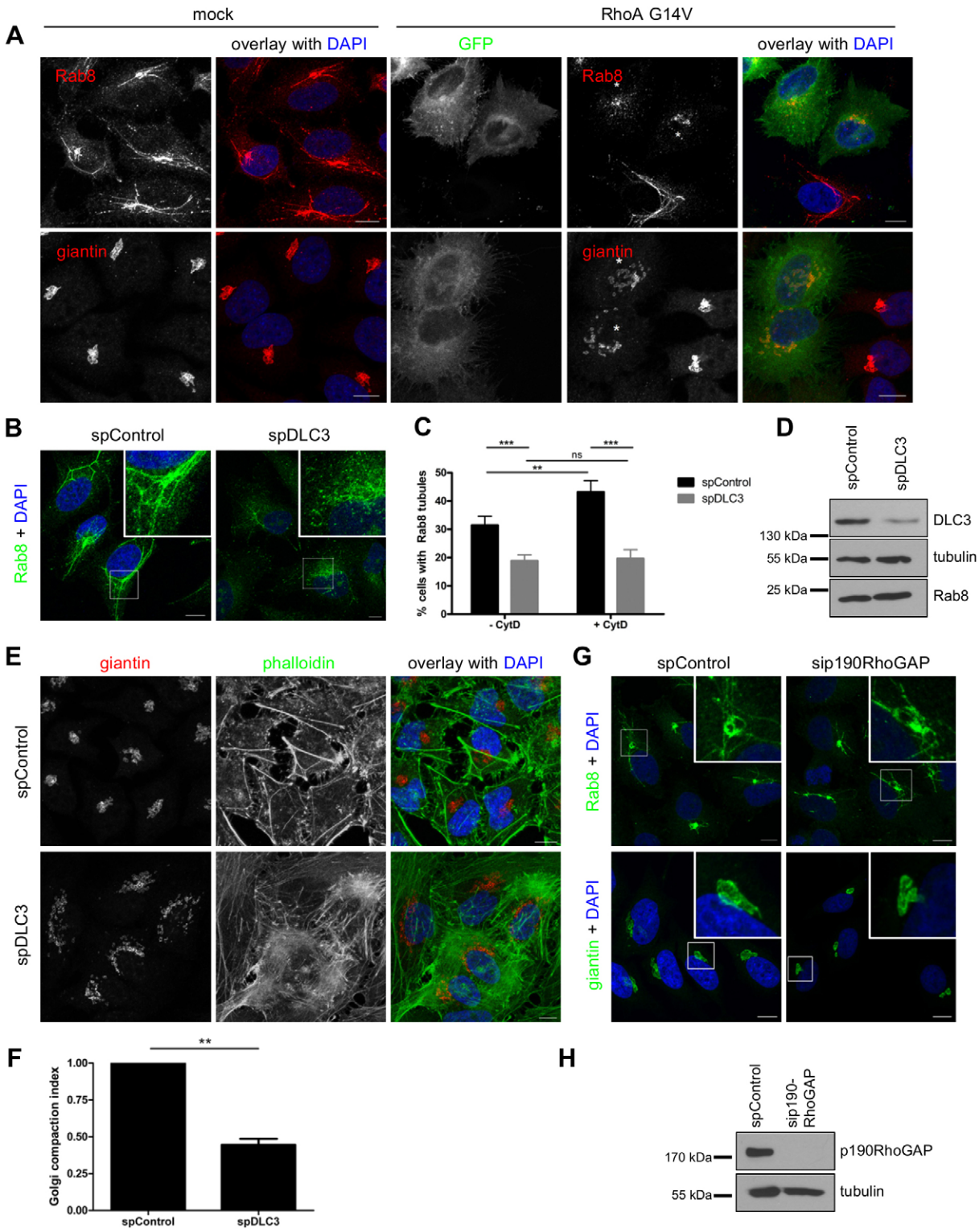

Fig. 3. See next page for legend.

immunoblotting (Fig. 3D). Endogenous Rab8 staining of control cells revealed prominent Rab8 tubules that originated from the perinuclear region (Fig. 3B). By contrast, DLC3-depleted cells showed a vesicular distribution of Rab8 in membrane protrusions and the perinuclear region. The number of cells displaying Rab8 tubules was significantly decreased by 30% and, in contrast to control cells, could not be enhanced by treatment with CytD (Fig. 3C). This could possibly be explained by a stabilized actin cytoskeleton, which was more resistant to CytD treatment (data not shown). Western blot analysis showed that Rab8 levels were not altered in DLC3-depleted cells (Fig. 3D), indicating a change in cellular distribution rather than expression.

Journal of Cell Science (2015) 128, 1386–1399 doi:10.1242/jcs.163857

Fig. 3. Both active RhoA and DLC3 depletion cause vesiculation of the Rab8 recycling compartment and Golgi fragmentation. (A) HeLa cells were either mock transfected or transfected with a plasmid encoding GFP–RhoA-G14V (green). The next day, cells were stained for Rab8 or giantin (red) and nuclei were counterstained with DAPI (blue). Note the dispersed morphology of the Rab8 compartment and Golgi complex in cells expressing constitutively active RhoA (*). (B–H) HeLa cells were transfected with control siRNA (spControl) or siRNAs specific for DLC3 (spDLC3) and p190RhoGAP-A (sip190RhoGAP), and analyzed 3 days later. (B) Cells were stained for Rab8 (green) and nuclei were counterstained with DAPI (blue). (C) Cells were left untreated or treated with 0.1 μM CytD. The number of cells containing Rab8-positive tubules was counted and normalized to the total number of analyzed cells. Data show the mean±s.e.m. ($n=3$, $N\geq100$ cells); ns, not significant; $^{**}P<0.001$; $^{***}P<0.0001$ (one-way ANOVA followed by Tukey's post-test). (D) Whole-cell lysates were analyzed by western blotting with anti-DLC3, anti-Rab8 and anti-tubulin antibodies. (E) Cells were stained for giantin (red), F-actin was labeled with phalloidin (green) and nuclei were counterstained with DAPI (blue). (F) The degree of Golgi fragmentation was quantified using the Golgi compaction index (Bard et al., 2003); values were normalized to the control. Data show the mean±s.e.m. ($n=3$, $N\geq40$ cells); $^{**}P=0.0053$ (paired Student's *t*-test). (G) Cells were stained for Rab8 and giantin (green), and nuclei were counterstained with DAPI (blue). (H) Whole-cell lysates were analyzed by western blotting with anti-p190RhoGAP and anti-tubulin antibodies. Scale bars: 10 μm.

Furthermore, the compact Golgi ribbon organization was lost in DLC3-depleted cells and single Golgi fragments were distributed throughout the cell, as visualized by giantin staining (Fig. 3E). The degree of Golgi dispersion was quantified using the Golgi compaction index (Bard et al., 2003). Compared with control cells, the value of this index dropped twofold in cells depleted of DLC3 (Fig. 3F). Fragmentation of the Golgi complex was not specific for either the cis or trans face and was also observed with the Golgi markers GM130 and p230 (also known as GOLGA2 and GOLGA4, respectively) (supplementary material Fig. S2B). Importantly, vesiculation of Rab8 recycling tubules and fragmentation of the Golgi complex were reproducible with an independent siRNA targeting DLC3 (supplementary material Fig. S2A,B). Moreover, DLC3 depletion induced the formation of actin stress fibers. Although actin cables in depleted cells were less thick than in control cells, they traversed the cytoplasm, forming a dense actin network (Fig. 3E). Immunostaining with the focal adhesion marker paxillin further revealed an accumulation of numerous focal adhesions at the tips of these actin-myosin bundles (supplementary material Fig. S3). These cytoskeletal changes were in accordance with the function of DLC3 as a RhoGAP protein and with increased Rho activity upon DLC3 knockdown.

Most probably owing to their short structure (Egea et al., 2013), we were unable to detect Golgi-associated actin microfilaments in both control and DLC3-depleted cells. Therefore, to rule out that vesiculation of the perinuclear region was a general consequence of RhoGAP downregulation, we depleted p190RhoGAP-A (also known as ARHGAP35) (Fig. 3H). This widely expressed RhoGAP has proven GAP specificity towards Rho and Rac (Settleman et al., 1992) and localizes to membrane ruffles as well as to adherens junctions (Arthur and Burridge, 2001; Wildenberg et al., 2006). In contrast to DLC3 downregulation, cells depleted of p190RhoGAP-A showed no obvious morphological changes in the Rab8 compartment or Golgi complex (Fig. 3G). Our findings thus support the hypothesis that vesiculation of the Rab8 and Golgi compartments are specific to DLC3 depletion and most likely a consequence of Rho hyperactivation.

DLC3 depletion enhances perinuclear RhoA activity

To investigate the spatial aspects of RhoA GTPase regulation by endogenous DLC3, we measured RhoA activity in DLC3-depleted HeLa cells using the RhoA biosensor, and we measured FRET over the whole cell by acceptor photobleaching. The FRET efficiency was then plotted as pseudocolor images representing high (red) and low (blue) RhoA activity (Fig. 4A). In control cells, high RhoA activity was observed near the plasma membrane (Fig. 4A) as reported previously (Pertz et al., 2006). Upon DLC3 depletion, RhoA activity was enhanced by 30% within the cell (Fig. 4B), with especially high levels of active RhoA in the perinuclear region (see pseudocolor image in Fig. 4A). Considering the reports on the localization of RhoA to the Golgi complex (Camera et al., 2003; Pertz et al., 2006) and the observed Golgi fragmentation upon loss of DLC3, we specifically measured RhoA activity at this compartment. The Golgi complex was visualized by co-staining of the cis- and medial-Golgi protein giantin using far-red-conjugated secondary antibodies that do not interfere with the FRET fluorophores. Quantification of RhoA activation at the Golgi complex, as well as the relative Golgi-localized RhoA activity, revealed a significant increase in DLC3-depleted cells compared to that of control cells (Fig. 4B). It is very likely that DLC3 loss also causes RhoA hyperactivation at the ERC; however, owing to the dispersion of the Rab8 compartment in DLC3-depleted cells, this subcellular site cannot easily be discerned. Importantly, enhanced total and Golgi-localized RhoA activity was also observed with an independent siRNA targeting DLC3 (supplementary material Fig. S2C,D), confirming the specificity of this effect.

A targeted DLC3 GAP domain rescues Golgi fragmentation

All DLC proteins possess a SAM domain, which potentially mediates protein–protein or protein–lipid interactions. To address whether this domain was involved in DLC3 recruitment to the Golgi–ERC interface, we expressed the isolated GFP-tagged DLC3α N-terminus (DLC3-SAM), which was found to accumulate in the perinuclear region (Fig. 5A). Interestingly, DLC3-SAM was not detected on Rab8-positive tubules, but extensively colocalized with TGN46 and giantin (Fig. 5A). To provide additional evidence that the SAM domain is necessary for the subcellular localization of DLC3, we ectopically expressed GAP-inactive DLC3β, an isoform that is generated by an alternative transcriptional start site and that naturally lacks the SAM domain (Durkin et al., 2007a). Indeed, DLC3β-K645E showed a cytosolic distribution without any colocalization with the Golgi complex or the Rab8 compartment (Fig. 5A; data not shown). The isolated SAM domain of DLC1 was fully cytosolic (Fig. 5A), indicating that the DLC3 SAM domain specifically determines the localization of this particular DLC isoform.

To prove that Golgi fragmentation was a consequence of local RhoA activation in DLC3-depleted cells, we designed a rescue experiment in which the DLC3-SAM was used to target DLC3 GAP activity to the Golgi complex. This was achieved by the direct fusion of the DLC3 GAP domain with DLC3-SAM. Fig. 5B shows a representative image of a DLC3-depleted cell expressing Golgi-localized, GFP-tagged SAM-GAP (Fig. 5B, marked with an asterisk). In contrast to untransfected cells, DLC3-depleted cells expressing SAM-GAP regained a compact Golgi complex (Fig. 5B, compare * and >), which was confirmed by quantification of the Golgi compaction index in these cells (Fig. 5C; see also supplementary material Fig. S2E for validation with an independent siRNA). No rescue of the Golgi compaction index was seen for DLC3-SAM alone (Fig. 5B,C). These results provide strong evidence that the RhoGAP activity

Journal of Cell Science (2015) 128, 1386–1399 doi:10.1242/jcs.163857

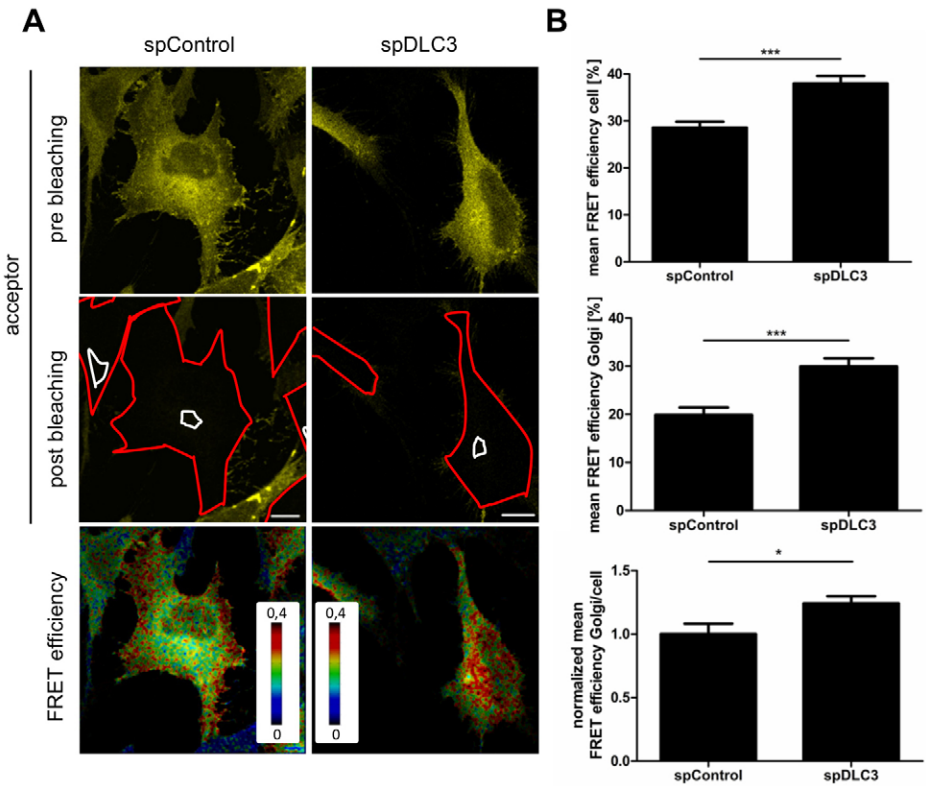

Fig. 4. DLC3 depletion enhances cellular RhoA activity. HeLa cells were transfected with control (spControl) or DLC3-specific (spDLC3) siRNAs. At 2 days post siRNA transfection, cells were co-transfected with the pTriEx-RhoA WT FLARE.sc biosensor and, on the next day, stained for giantin. (A) Pre- and post-bleach images of the acceptor (YFP) are depicted. Red lines denote the region of interest (ROI) where the acceptor was bleached; white lines represent the Golgi ROI. FRET efficiencies are displayed as a pseudocolor thermal map corresponding to the depicted scale, from low (blue) to high (red) RhoA activity. Scale bars: 5 µm. (B) Plotted are the mean FRET efficiencies within the cell and at the Golgi complex, as well as the Golgi:cell (Golgi/cell) ratio. Results of the cells from two independent experiments are depicted as the mean±s.e.m. ($N \geq 40$ cells); *$P=0.0244$; ***$P<0.0001$ (unpaired Student's *t*-test).

of DLC3 indeed limits RhoA activation at the Golgi complex and most likely at the ERC.

DLC3 is required for transferrin trafficking to the ERC

Upon internalization, transferrin (Tfn) is delivered to early endosome antigen 1 (EEA1)-positive endosomes from where it is transported to the ERC to then recycle back to the plasma membrane through the Rab11-dependent slow recycling pathway (Grant and Donaldson, 2009). To address whether DLC3 affects ERC function, we first measured Tfn recycling by pulse-chase experiments. Cells were pulsed with Alexa-Fluor-555-labeled Tfn (Tfn–555) for 1 h and the fluorescence intensity of chased cells was then determined by flow cytometric analysis. In both control and DLC3-depleted cells, the loss of internal fluorescence was similar (Fig. 6A), indicating that the rate at which Tfn recycles to the plasma membrane is unchanged upon DLC3 depletion. Previously, Rab8 was found to be important for the delivery of internalized Tfn to the ERC, but not for Tfn internalization or recycling from the ERC to the plasma membrane (Hattula et al., 2006). We therefore addressed whether DLC3 affects the subcellular distribution of internalized Tfn. After a 1-h incubation, Tfn was transported to the perinuclear region in control cells (Fig. 6B). By contrast, DLC3-depleted cells showed a dispersed localization of Tfn accumulating in large vesicles that were localized in the cell periphery (Fig. 6B,C). Western blot analysis revealed similar total transferrin receptor (TfnR) levels in control and DLC3-depleted cells; in addition, similar levels of surface-bound Tfn were measured by flow cytometry (Fig. 6D), excluding differences in Tfn uptake due to varying TfnR levels. Immunostaining analysis revealed that internalized Tfn in DLC3-depleted cells strongly colocalized with EEA1, whereas at this time-point of uptake, control cells showed only little overlap of Tfn with EEA1 (Fig. 6B). Moreover, we found that the early endosomes in depleted cells were enlarged compared with those of control cells (Fig. 6B) and that internalized Tfn strongly colocalized with overexpressed GFP-tagged Rab4 (Fig. 6E), a Rab GTPase that mediates fast endocytic recycling directly from early endosomes (Stenmark, 2009). Although overall Tfn recycling kinetics were similar, our findings on the impaired Tfn delivery from early endosomes to the ERC and its presence in Rab4-positive vesicles indicate that DLC3 loss leads to altered endosomal cargo routing.

We next analyzed whether the defect in Tfn localization upon DLC3 depletion was Rho dependent. Depletion of DLC3 together with RhoA only partially restored Tfn accumulation at the ERC (Fig. 6F). This is most likely due to the compensatory upregulation of RhoB upon RhoA knockdown (Fig. 6G), which was observed previously (Ho et al., 2008; Vega et al., 2011). Furthermore, it has been suggested that constitutively active RhoB prevents endosomal transport (Fernandez-Borja et al., 2005) and, indeed, downregulation of RhoB in DLC3-depleted cells also led to a partial rescue of the Tfn transport to the perinuclear region (Fig. 6F). Importantly, although the knockdown was not complete, the simultaneous suppression of RhoB expression in DLC3- and RhoA-depleted cells completely restored Tfn transport to the ERC, whereas depletion of RhoA and RhoB alone had no effect (Fig. 6F,G). DLC3 thus regulates endosomal Tfn trafficking by the regulation of RhoA and most likely also RhoB, when taking into account the colocalization of DLC3 with endosomal RhoB (supplementary material Fig. S1D).

DLC3 regulates EGFR endocytosis and signaling

The EGFR is a receptor tyrosine kinase that is rapidly endocytosed upon EGF ligand binding and is transported to lysosomes in a RhoB-dependent manner. Active RhoB was shown to delay the intracellular trafficking of the EGFR and its

Journal of Cell Science (2015) 128, 1386–1399 doi:10.1242/jcs.163857

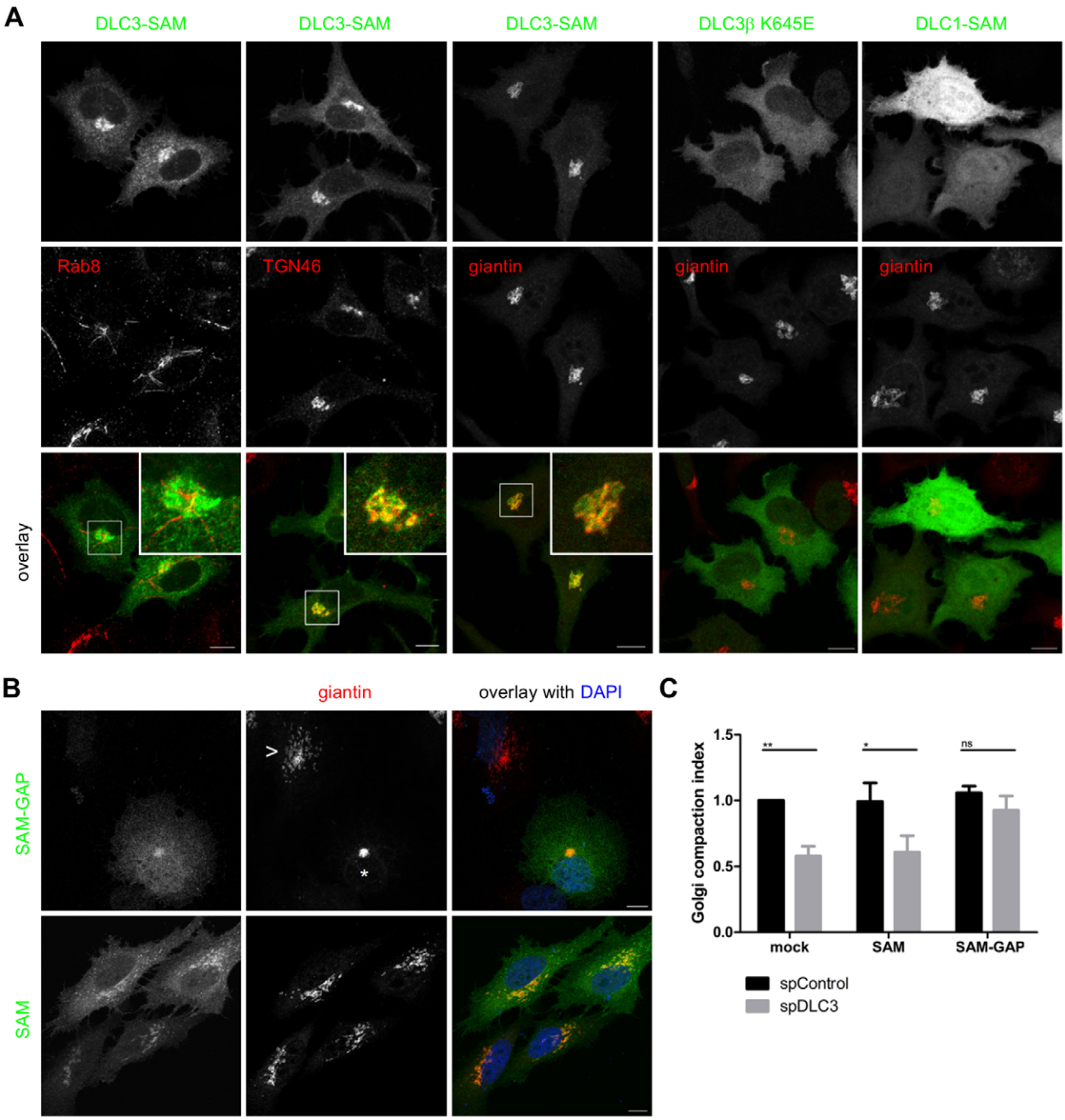

Fig. 5. DLC3-SAM localizes to Golgi membranes and the targeted DLC3 GAP domain rescues Golgi fragmentation in DLC3 knockdown cells. (A) HeLa cells transiently expressing GFP-tagged DLC3-SAM, GFP-tagged DLC3β-K645E or mCherry-tagged DLC1-SAM (all depicted in green) were stained for Rab8, TGN46 or giantin (red) as indicated. (B,C) HeLa cells were transfected with control (spControl) or DLC3-specific (spDLC3) siRNAs. At 2 days post siRNA transfection, cells were transfected with vectors encoding the DLC3 GAP domain fused to DLC3-SAM (SAM-GAP) or DLC3-SAM alone (SAM). Cells were fixed and stained for giantin 24 h later. (B) Representative maximum projections of DLC3-depleted cells are shown. Note the morphological difference of giantin (red) in untransfected cells (>) compared to SAM-GAP-expressing (green) cells (*). Nuclei were counterstained with DAPI (blue). Scale bars: 10 µm. (C) The Golgi compaction index was calculated for at least three independent experiments. Values were normalized to untransfected control cells and are depicted as the mean±s.e.m. (n=3–6, $N\geq50$ cells); ns, not significant; *$P<0.05$; **$P<0.01$ (two-way ANOVA followed by Bonferroni post-test).

lysosomal degradation (Gampel et al., 1999). To analyze how EGFR trafficking might be affected by DLC3 downregulation and subsequent Rho misregulation, we incubated cells with Alexa-Fluor-555-labeled EGF (EGF–555) for different lengths of time. After 20 min, EGF-positive endosomes were primarily localized in the perinuclear region in control cells, whereas, in DLC3-depleted cells, EGF–555 accumulated in enlarged EEA1-positive endosomes in the cell periphery (Fig. 7A). Although the levels of internalized EGF were comparable between control and depleted cells, we found significantly more peripheral EGF–555 localization upon DLC3 depletion (Fig. 7B). After 40 min, EGF–555 still failed to accumulate in the perinuclear region in

Journal of Cell Science (2015) 128, 1386–1399 doi:10.1242/jcs.163857

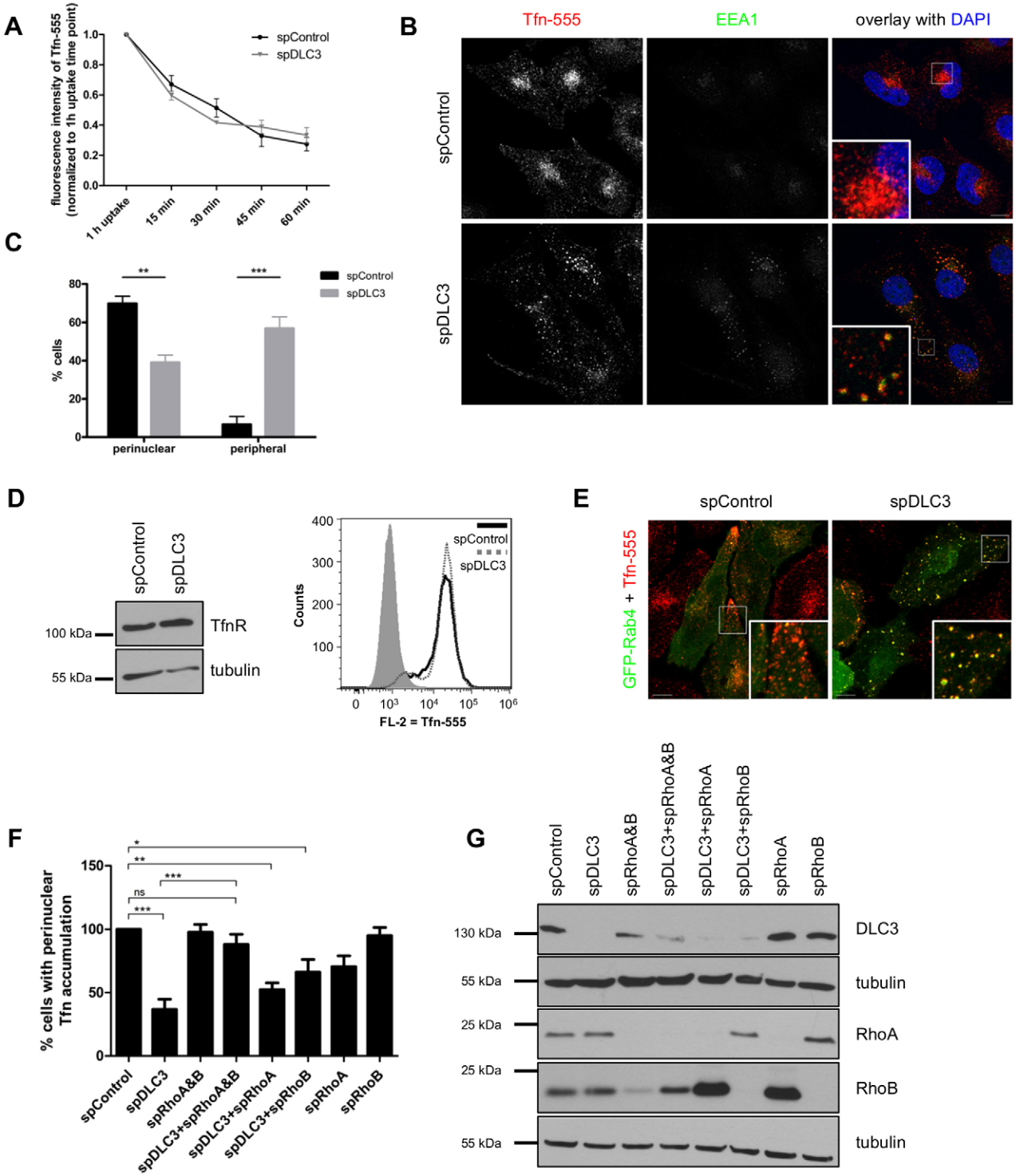

Fig. 6. See next page for legend.

DLC3-depleted cells (Fig. 7A), indicating that EGF–555 was not delivered to later endosomal compartments. Indeed, after 120 min, DLC3-depleted cells showed a significant pool of remaining EGF–555, whereas the signal was strongly reduced in control cells (Fig. 7C,D). This remaining EGF–555 pool did not colocalize with the late endosomal and lysosomal marker LAMP1 (Fig. 7C), excluding incomplete EGF–555 degradation due to lysosomal dysfunction. To further investigate the identity of the remaining EGF pool in DLC3-depleted cells, we performed immunostaining analysis of different Rab recycling markers. At 120 min post-internalization, EGF–555 in DLC3-depleted cells colocalized with neither EEA1 nor Rab7 (supplementary material Fig. S4A), but extensively overlapped with GFP-tagged Rab4 (Fig. 7E). DLC3 depletion thus impairs EGFR lysosomal degradation and, reminiscent of the TfnR, appears to cause receptor re-routing to the Rab4-dependent recycling pathway.

Fig. 6. DLC3 depletion impairs Tfn transport to the ERC. (A–E) HeLa cells were transfected with control (spControl) or DLC3-specific (spDLC3) siRNAs and analyzed 3 days later. (A) Serum-starved cells were incubated with Tfn–555 for 1 h (pulse) and then chased for the indicated times. The decrease in Tfn–555 fluorescence intensity was measured by flow cytometry, and two representative experiments are depicted as the mean±s.e.m. (B,C) Serum-starved cells were incubated with Tfn–555 (red) for 1 h and stained for EEA1 (green). Representative maximum projections are shown and imaging parameters were identical. Scale bars: 10 µm. (C) The number of cells displaying Tfn–555 either at the perinuclear region or in the cell periphery was counted and normalized to the total number of analyzed cells. Data show the mean±s.e.m. ($n=3$, $N\geq36$ cells); $^{**}P<0.01$; $^{***}P<0.001$ (two-way ANOVA followed by Bonferroni post-test). (D) Left panel, whole-cell lysates were analyzed by western blotting with anti-TfnR and anti-tubulin antibodies. Right panel, flow cytometric analysis of surface-bound Tfn. Unlabeled cells are shown filled in gray. (E) At 2 days post siRNA transfection, cells were transfected with a vector encoding GFP–Rab4-WT (green). The next day, serum-starved cells were incubated with Tfn–555 (red) for 1 h. Scale bars: 10 µm. (F,G) HeLa cells were transfected with control siRNAs (spControl) or siRNAs specific for DLC3 (spDLC3), RhoA (spRhoA) and RhoB (spRhoB), and analyzed 3 days later. (F) Serum-starved cells were incubated with Tfn–555 for 1 h. The percentage of cells displaying Tfn–555 at the perinuclear region was determined and normalized to the control. Data show the mean±s.e.m. ($n=3$, $N\geq50$ cells); ns, not significant; $^{*}P<0.01$; $^{**}P<0.001$; $^{***}P<0.0001$ (one-way ANOVA followed by Tukey's post-test). (G) Whole-cell lysates were analyzed by western blotting with anti-DLC3, anti-RhoA, anti-RhoB and anti-tubulin antibodies.

Because the receptor trafficking route determines the signaling response, we examined EGFR levels and activity by immunoblotting cell lysates of EGF-stimulated HeLa cells. Basal EGFR levels of DLC3-depleted cells were comparable to those of control cells (Fig. 8A; EGFR). Immediately after EGF stimulation, strong phosphorylation of EGFR at Tyr1068 was detected in both control and depleted cells (Fig. 8A; pEGFR). After 15 min of stimulation, the level of EGFR was already decreased in control cells, whereas even at late time points the receptor levels persisted in DLC3-depleted cells (Fig. 8A, EGFR; Fig. 8B for quantification). EGFR activation triggers downstream signaling, including the activation of the PI3K and MAPK pathways, resulting in the activation of AKT and ERK kinases, respectively. Compared with control cells, the total levels of these kinases were reduced in DLC3-depleted cells for unknown reasons (Fig. 8A; AKT and ERK). Nevertheless, correlating with the delayed EGFR degradation, phosphorylation and thus activation of AKT was prolonged in DLC3-depleted cells (Fig. 8A; pAKT). In the breast cancer cell line MCF7, prolonged AKT and also ERK phosphorylation were observed, indicating that this effect is not restricted to a particular cell line (supplementary material Fig. S4B; note that the levels of the EGFR itself are too low for detection by immunoblotting). Thus, given its potential tumor suppressor function, the ability of DLC3 to regulate EGFR degradation could be one mechanism by which DLC3 loss contributes to cancer progression.

DISCUSSION

Here, we establish a novel role for the RhoGAP protein DLC3 in the control of endocytic vesicle traffic. DLC3 is shown to localize at the interface of the TGN and Rab8-positive recycling compartment where it regulates RhoA activity. In the absence of DLC3, the structural integrity of the Golgi complex and Rab8 compartment are compromised, most likely owing to the induction of aberrant cytoskeletal rearrangements. Both the actin and microtubule cytoskeleton play important roles in the maintenance of organelle morphology and positioning (Egea et al., 2013; Yadav and Linstedt, 2011). Downstream of active RhoA, the Rab8-positive ERC dispersed, which is in line with the RhoA-mDia-induced Golgi fragmentation mediated by actin polymerization, myosin-II-driven contractility and microtubule-dependent movement (Zilberman et al., 2011), highlighting the necessity of tight control of Rho signaling. To the best of our knowledge, our study identifies DLC3 as the first Rho-specific GAP protein in living cells that maintains the structure and function of the ERC and Golgi compartments.

The specific colocalization of DLC3 with Rab8 and the impact of DLC3 expression on the formation of Rab8-positive tubules suggest a role for DLC3 in Rab8-dependent processes. Rab8 and Rab11 are both found at the ERC where the two GTPases control different steps in the recycling of Tfn. Whereas Rab11 regulates Tfn recycling from the ERC to the plasma membrane, Rab8 controls the delivery of Tfn to the perinuclear ERC (Hattula et al., 2006; Roland et al., 2007; Ullrich et al., 1996). Our findings on the impaired Tfn delivery to the ERC in DLC3-depleted cells, in which Tfn accumulated in enlarged EEA1-positive endosomes in the cell periphery, are in agreement with these differential Rab functions. Considering that the actin depolymerizing agent CytD enhances Rab8 tubulation, the right balance of actin polymerization and depolymerization appears to be crucial for the biogenesis of Rab8-positive transport carriers. We therefore propose that increased local Rho signaling in the absence of DLC3 triggers the loss of Rab8 recycling tubules, causing a transport block at the early endosomal stage. Because Rab8a/b, together with Rab10 and Rab13, compose a subfamily of closely related Rab proteins with overlapping localizations and functions (Stenmark, 2009), it is possible that DLC3 affects additional Rabs. Our observation on the compact appearance of both Rab8 and Rab11 in DLC3-WT-expressing cells might also suggest a role of DLC3 in Rab11-dependent recycling processes.

The endosomal Tfn transport block in DLC3-depleted cells was fully rescued by the simultaneous knockdown of RhoA and RhoB, demonstrating the involvement of Rho hyperactivation. The compensatory upregulation of RhoB in cells lacking RhoA provides an explanation for why RhoA knockdown alone only partially restored Tfn transport in these cells. Considering the colocalization of DLC3-K725E with endosomal RhoB, DLC3 is likely to possess RhoB-inhibitory activity too. Unfortunately, biochemical pulldown assays failed to reveal the potential RhoB regulation by DLC3, making the development of a RhoB biosensor necessary to address this question at the subcellular level. Because retrograde and anterograde transport processes are intimately connected to ensure cellular homeostasis, any defects at the level of endosomal recycling are likely to affect Golgi integrity and vice versa. This is supported by our observation that overexpression of inactive Rab8a negatively affected Golgi compaction (data not shown). There are also hints for the direct regulation of TGN function by Rho signaling, as myosin II and actin were found to play an important role in the fission of Rab6 vesicles (Miserey-Lenkei et al., 2010). Furthermore, the actin-severing protein actin-depolymerizing factor (ADF)/cofilin and its upstream regulator LIM kinase 1 were reported to regulate fission and cargo sorting at the TGN (von Blume et al., 2009; Salvarezza et al., 2009). Although TGN46 and Rab6 did not accumulate on the tubular structures positive for GAP-inactive DLC3, DLC3 might be still involved in controlling the formation of a specific subset of transport carriers from the TGN by local Rho regulation.

Journal of Cell Science (2015) 128, 1386–1399 doi:10.1242/jcs.163857

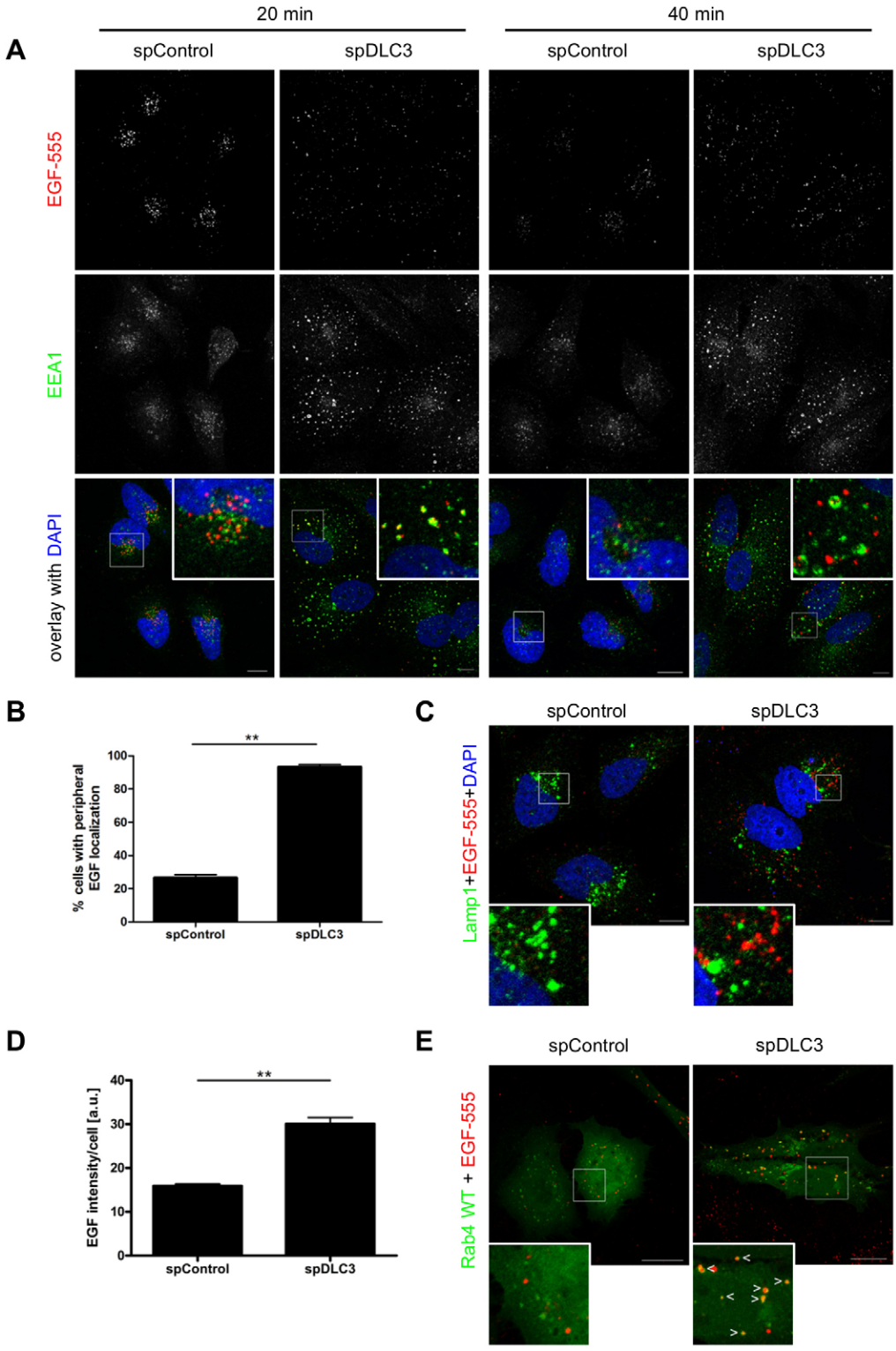

Fig. 7. DLC3 depletion impairs degradation of activated EGFR. HeLa cells were transfected with control (spControl) or DLC3-specific (spDLC3) siRNAs. (A,B) At 3 days post siRNA transfection, cells were incubated with EGF–555 (red) for 20 and 40 min, and stained for EEA1 (green). Nuclei were counterstained with DAPI (blue). (B) The number of cells displaying EGF–555 in the cell periphery after a 20-min incubation was counted and normalized to the total number of analyzed cells. Data show the mean±s.e.m. (n=3, N=50 cells); $^{**}P$=0.0013 (paired Student's t-test). (C,D) At 3 days post siRNA transfection, cells were incubated with EGF–555 (red) for 120 min and stained for Lamp1 (green). Nuclei were counterstained with DAPI (blue). (D) Quantification of the mean fluorescence intensity of EGF–555 per cell after incubation for 120 min. Data show the mean±s.e.m. (n=3, N=50 cells); $^{**}P$=0.0066 (paired Student's t-test). (E) At 2 days post siRNA transfection, cells were transfected with a vector encoding GFP–Rab4-WT (green). The next day, cells were incubated with EGF–555 (red) for 120 min. Note the overlapping distribution of EGF–555 and GFP–Rab4 (>). (A,C,E) Representative maximum projections are shown and imaging parameters were identical. Scale bars: 10 µm.

Targeted expression of the isolated DLC3 GAP domain was sufficient to restore Golgi compaction in DLC3-depleted cells, providing clear evidence for a GAP-dependent Rho regulatory mechanism. Although the SAM domain of DLC1 and DLC3 are highly conserved (Durkin et al., 2007a), the isolated SAM domain of DLC1 did not localize to the Golgi complex, but was fully cytosolic. These differences support the idea that the DLC family members exert isoform-specific functions associated with their distinct localizations, ultimately resulting in distinct spatiotemporal Rho activation patterns. Interestingly, DLC3-SAM did not overlap with Rab8-positive structures, indicating that additional domains are required for the transport of DLC3 itself from the Golgi membranes to the ERC. Considering the localization at the Golgi complex, the ERC, endocytic vesicles

Journal of Cell Science (2015) 128, 1386–1399 doi:10.1242/jcs.163857

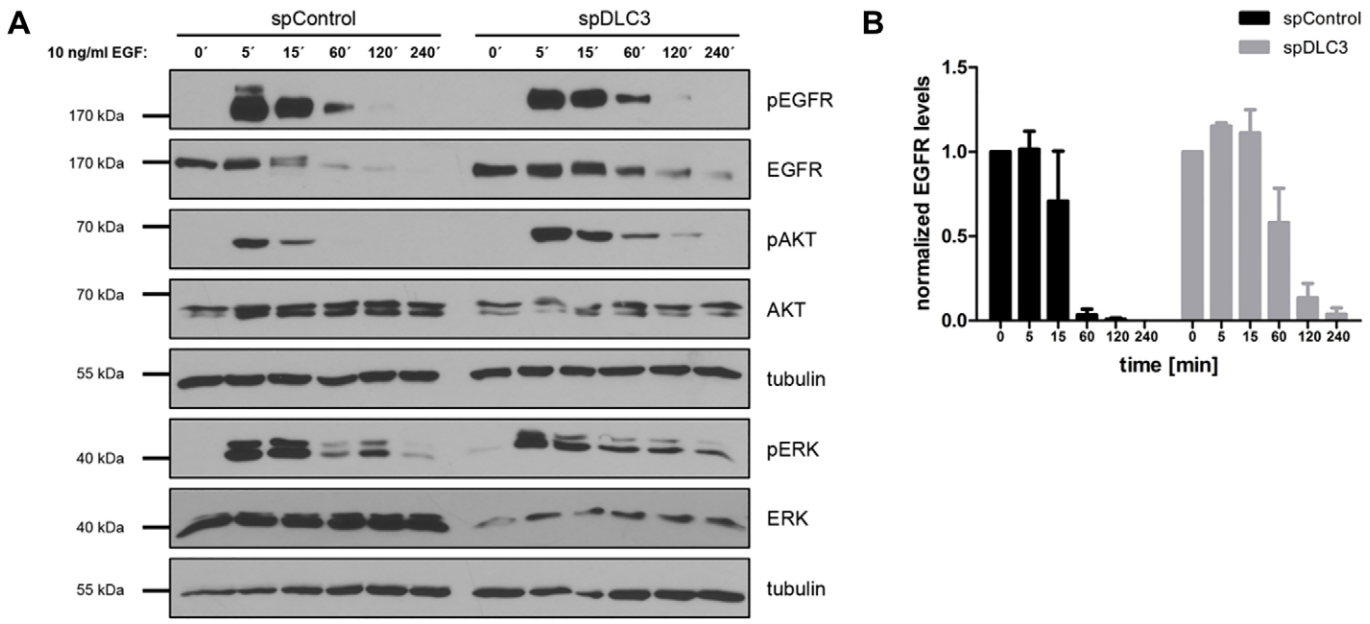

Fig. 8. DLC3 depletion prolongs EGFR signaling. HeLa cells were transfected with control (spControl) or DLC3-specific (spDLC3) siRNAs. At 2 days post siRNA transfection, cells were serum starved overnight and, prior to lysis, stimulated with 10 ng/ml EGF for the indicated times. (A) Whole-cell lysates were analyzed by western blotting with anti-pEGFR (Tyr1068), anti-EGFR, anti-pAKT (Thr308), anti-AKT, anti-pERK (Thr202/Tyr204), anti-ERK and anti-tubulin antibodies. (B) EGFR levels from two independent experiments including the blot shown in A were quantified and normalized to tubulin. Data show the mean±s.e.m.

and cell–cell contacts (Holeiter et al., 2012), DLC3 appears to dynamically associate with different cellular membranes, where it might exert GAP-dependent and perhaps also GAP-independent functions.

We further provide evidence that DLC3 is required for the proper lysosomal degradation of the EGFR. In the absence of DLC3, the EGFR accumulated in Rab4-positive vesicles. Similarly, in DLC3-depleted cells, internalized Tfn was found to colocalize with Rab4, which is responsible for the fast recycling of cargo. This is in line with the observation that disturbed ERC integrity can lead to missorting of endocytosed Tfn (Hattula et al., 2006; Horgan et al., 2007; Naslavsky et al., 2006). In the case of the EGFR, disruption of the ERC by overexpression of the clathrin adaptor protein Eps15S (a short form of Eps15) caused the accumulation of the EGFR in early endosomes and potentiated receptor recycling (Chi et al., 2011). Although receptor internalization is a mechanism by which receptor signaling is terminated, it is now widely accepted that endosomes constitute active signaling platforms (Platta and Stenmark, 2011; Tomas et al., 2014), and, indeed, endosomal accumulation of EGF-stimulated EGFR in DLC3-depleted cells was associated with prolonged AKT activation. The selective activation of AKT might be mediated by the Rab5 effector protein APPL1 that regulates AKT activation from endosomes (Schenck et al., 2008).

It is tempting to speculate that the regulation of the turnover of membrane receptors and membrane-proximal signaling molecules by DLC3 might not be restricted to the EGFR. We previously reported that, in MCF7 and MCF10A breast epithelial cells, DLC3 predominantly localizes to cell–cell contacts. In the absence of DLC3, the adherens junction proteins E-cadherin and β-catenin were mislocalized, which was associated with enhanced migration and increased cell disaggregation (Holeiter et al., 2012). Given its novel function in membrane transport, DLC3 might also be involved in the regulation of the trafficking of adherens junction proteins. Intriguingly, Rab8 was found to regulate E-cadherin transport by binding to the JRAB (also known as MICAL-L2) effector protein (Yamamura et al., 2008). DLC3 might thus possess a more global role in membrane trafficking through the integration of Rho and Rab GTPase signaling. Our future studies will focus on defining the molecular factors that regulate DLC3 activity and localization. In particular, it will be interesting to identify protein and/or lipid interactors of DLC3 that recruit the protein to the different subcellular compartments and to delineate in more detail the downstream effector pathways that govern its function. The increased understanding of DLC3 biology will also shed light onto its potential function in the suppression of the different steps of neoplastic cell transformation.

MATERIALS AND METHODS

Cell culture

HeLa cells (ATCC; Manassas, VA) and MCF7 cells (kindly provided by Cornelius Knabbe; Institute of Clinical Pharmacology, Stuttgart, Germany) were grown and maintained in RPMI 1640 (Invitrogen; Carlsbad, CA) supplemented with 10% FCS (PAA Laboratories; Cölbe, Germany) at 37℃ and 5% CO_2.

Antibodies and reagents

The antibodies used were as follows: monoclonal mouse anti-GM130, monoclonal mouse anti-p230, monoclonal mouse anti-paxillin and monoclonal mouse anti-p190RhoGAP antibodies from BD Transduction Laboratories (Heidelberg, Germany); polyclonal rabbit anti-giantin (ab24586) antibodies from Abcam (Cambridge, UK); monoclonal rabbit anti-Rab8 (D22D8), polyclonal rabbit anti-Rab7, polyclonal rabbit anti-Rab6 (D37C7), polyclonal rabbit anti-EEA1, monoclonal rabbit anti-pAKT (Thr308; C31E5E), monoclonal mouse anti-AKT (pan; 40D4), monoclonal rabbit anti-pEGFR (Tyr1068; D7A5), polyclonal rabbit anti-pERK1/2 (Thr202/Tyr204), monoclonal mouse anti-ERK1/2 (3A7) and polyclonal rabbit anti-RhoB antibodies from Cell Signaling (Cambridge, UK); monoclonal mouse anti-TfnR antibodies

from Invitrogen; monoclonal mouse anti-Lamp1 antibodies from Developmental Studies Hybridoma Bank (University of Iowa; IA); sheep serum antibodies recognizing TGN46 (AHP500) from BioRad Laboratories (Hercules, CA); monoclonal mouse anti-α-tubulin and monoclonal anti-FLAG M2 antibodies from Sigma-Aldrich (St Louis, MO); monoclonal mouse anti-DLC3 (E-2), monoclonal mouse anti-RhoA (26C4) and polyclonal rabbit anti-EGFR (1005) antibodies from Santa Cruz Biotechnology (Dallas, TX). Horseradish peroxidase (HRP)-labeled secondary anti-mouse- and anti-rabbit-IgG antibodies were obtained from GE Healthcare (Piscataway, NJ), Alexa-Fluor®-labeled secondary IgG antibodies and Alexa-Fluor®-labeled phalloidin were obtained from Invitrogen. Alexa-Fluor®-labeled phalloidin was obtained from Invitrogen. DAPI was obtained from Sigma-Aldrich. CytD was obtained from Enzo Life Sciences (Lörrach, Germany) and EGF was from R&D Systems (Minneapolis, MN).

DNA constructs and transfection

The expression vectors pEGFP-C1-DLC3α-WT, pEGFP-C1-DLC3α-K725E, pEGFP-C1-DLC3β-K645E and pmCherry-C1-DLC3α-K725E have been described previously (Erlmann et al., 2009; Holeiter et al., 2012). pCR.V62-Met-FLAG-DLC3α-WT and K725E were generated by *Eco*RI excision of the DLC3 cDNAs from pEGFP vectors (Erlmann et al., 2009; Holeiter et al., 2012) and cloning into the pCR.V62-Met-FLAG vector. pEGFP-C1-DLC3-SAM (encoding the first 80 amino acids in DLC3α) was generated by PCR amplification using pEGFP-C1-DLC3α as a template and the following forward and reverse primers: 5′-CCGGAATTCTCCTCTGCTGGACGTTTTCTG-3′ and 5′-CCGGAATTCTCACAGCCTCCTACACAGGGC-3′. The PCR product was cloned into the pEGFP-C1 vector by *Eco*RI restriction. pmCherry-C1-DLC1-SAM was subcloned from pEGFP-C1-DLC1-SAM (Heering et al., 2009) by *Bgl*II/*Bam*HI and *Sal*I/*Xho*I restriction into the pmCherry-C1 vector. pEGFP-C1-DLC3-SAM-GAP was generated in two steps. First, the sequence encoding amino acids 1–80 was amplified by PCR without integration of a stop codon using pEGFP-C1-DLC3α as a template and the following forward and reverse primers: 5′-CCGGAATTCTCCTCTGCTGGACGTTTTCTG-3′ and 5′-GCAGTCGACCAGGCCTCCTACACAGGGC-3′. The PCR product was cloned into the pEGFP-C1 vector by *Eco*RI and *Sal*I restriction. Next, the GAP domain was amplified by PCR using pEGFP-C1-DLC3α as a template and the following forward and reverse primers: 5′-GCAGTCGACAAGGGCTCACTGCTGCGGC-3′ and 5′-GCAGTCGACTCACTGACGCAGCTCAGCCAGG-3′. This PCR product was cloned into the pEGFP-C1-DLC3-SAM vector lacking the stop codon by *Sal*I restriction. To obtain pEGFP-C1-RhoA-G14V, the RhoA-WT expression cassette was subcloned from pcDNA3.1-HA-RhoA-WT by *Bgl*II/*Bam*HI and *Eco*RI restriction into the pEGFP-C1 vector. Next, the G14V mutation was introduced by site-directed PCR mutagenesis using the following forward primer: 5′-GTGATTGTTGGTGATGTAGCCTGTGGAAAGACA-3′. All amplified cDNAs were verified by sequencing. Oligonucleotides were purchased from Eurofins MWG Operon (Ebersberg, Germany). The RhoA-WT biosensor pTriEx-RhoA FLARE.sc was purchased from Addgene (Addgene plasmid 12150; Pertz et al., 2006). The pECFP-RhoB/Endo vector was purchased from Clontech (Clontech plasmid #6934-1). pEGFP-Rab11 and pEGFP-Rab4 vectors were kindly provided by Lucas Pelkman (University of Zurich, Switzerland) and Hesso Farhan (University of Konstanz, Germany), respectively. Vector transfections were carried out with TransIT-HeLaMONSTER® (Mirus Bio; Madison, WI) and Turbofect® (Thermo Scientific; Rockford, IL), according to the manufacturer's instructions.

RNA interference

For RNA interference, cells were reverse transfected with siRNAs using Lipofectamine® RNAiMAX (Invitrogen) according to the manufacturer's instructions. As a negative control (termed spControl), ON-TARGETplus® non-targeting control pool D-001810-10 from Dharmacon (Lafayette, CO) was used. Two independent DLC3-specific siRNAs were used, termed spDLC3 and siDLC3. spDLC3 corresponds to the siGENOME SMARTpool human STARD8 M-010254 from Dharmacon. siDLC3 corresponds to a single duplex with the sense sequence: 5′-UCUC-UGAGGCGGAAGGAAA-3′ (Eurofins MWG Operon). sip190RhoGAP corresponds to a single duplex with the sense sequence 5′-GGAU-UGUGUGGAAUGUAAG-3′ (Eurofins MWG Operon). spRhoA and spRhoB correspond to the ON-TARGETplus® SMARTpool human RhoA L-003860 and ON-TARGETplus® SMARTpool human RhoB L-008395 from Dharmacon, respectively.

Cell lysis, SDS-PAGE and western blotting

Cells were washed once with PBS and lysed for 10 min with ice-cold RIPA buffer [50 mM Tris-HCl pH 7.5, 150 mM sodium chloride, 1% (v/v) NP-40, 0.25% (v/v) sodium deoxycholate, 0.1% (v/v) SDS, 1 mM EDTA, 1 mM sodium orthovanadate, 10 mM sodium fluoride, 0.5 mM PMSF and 20 mM β-glycerophosphate plus protease inhibitors]. Whole-cell lysates were clarified by centrifugation for 10 min at 15,700 ***g*** and 4℃. Equal amounts of protein were loaded on 8% or 15% polyacrylamide gels and transferred to polyvinylidene difluoride membranes (Roth; Karlsruhe, Germany). For detection of RhoA and RhoB, lysates were run on NuPage® Novex® 4–12% Bis-Tris gels (Invitrogen) and blotted onto nitrocellulose membranes using the iBlot® device (Invitrogen). Membranes were blocked for 30 min with 0.5% (v/v) blocking reagent (Roche Diagnostics; Mannheim, Germany) in PBS containing 0.05% (v/v) Tween-20 and 0.01% (v/v) thimerosal. Membranes were incubated with primary antibodies overnight at 4℃, followed by 1 h incubation with HRP-conjugated secondary antibodies at room temperature. Proteins were visualized using an enhanced chemiluminescence detection system (Thermo Scientific; Rockford, IL). Quantification of ECL films was performed by densitometric analysis using ImageJ software (NIH; Bethesda, MD).

Immunofluorescence staining and confocal microscopy

Cells grown on glass coverslips coated with 10 µg/ml collagen R (Serva; Heidelberg, Germany) were fixed for 15 min with 4% (v/v) paraformaldehyde. After washes in PBS, cells were incubated for 15 min with 150 mM glycine in PBS and permeabilized for 5 min with 0.1% (v/v) Triton X-100 in PBS. Blocking was performed with 5% (v/v) goat serum (Invitrogen) in PBS containing 0.1% (v/v) Tween-20. Fixed cells were incubated with primary antibodies diluted in blocking buffer for 2 h at room temperature. Following three washing steps with PBS, cells were incubated with Alexa-Fluor®-(488, 546 or 633)-labeled secondary antibodies in blocking buffer for 1 h at room temperature. Nuclei were counterstained with DAPI and coverslips were mounted in Fluoromount-G® (SouthernBiotech; Birmingham, AL). All samples were analyzed at room temperature using a confocal laser scanning microscope (LSM 710, Carl Zeiss; Oberkochen, Germany) equipped with a Plan Apochromat 63×/1.40 DIC M27 (Carl Zeiss) oil-immersion objective. Linear adjustments to brightness, contrast and maximum intensity projections were made using the ZEN software (Carl Zeiss). For quantification of mean fluorescence intensities, images were acquired with the same confocal settings and analyzed using the ImageJ software (NIH; Bethesda, MD). Fluorescence intensities along a line of interest were measured using the ZEN software. For colocalization and line-scan experiments, all images were acquired with identical dimensions in *x* and *y* directions and the same pinhole settings (1 AU in the red channel). The fraction of Rab8 staining overlapping with DLC3-K725E signals was analyzed using the ImageJ plugin JACoP, measuring the Manders' M2 coefficient (Bolte and Cordelières, 2006).

FRET analysis

For FRET measurements, cells were transfected overnight with the RhoA-WT biosensor pTriEx-RhoA FLARE.sc and pCR.V62-Met-FLAG, pCR.V62-Met-FLAG-DLC3α-WT or pCR.V62-Met-FLAG-DLC3α-K725E. The next day, cells were fixed and immunostained with anti-Flag M2 and Alexa-Fluor®-633-labeled secondary anti-mouse antibodies. In the case of siRNA transfection, control and DLC3-depleted cells were co-transfected with the RhoA-WT biosensor at 2 days post siRNA transfection and, the next day, cells were fixed and immunostained for the cis- and medial-Golgi marker giantin using an Alexa-Fluor®-633-labeled secondary

anti-mouse-IgG antibody. The staining was performed according to the immunofluorescence staining protocol described above and samples were then mounted in Mowiol® (Polysciences; Warrington, PA) mounting solution. FRET efficiencies were determined using the acceptor photobleaching method. CFP was excited with a diode UV laser at 405 nm, and emission was detected in the spectral window 454–515 nm. YFP was excited with the 514-nm laser line of an argon laser and emission was detected from 515–621 nm. Donor and acceptor images were acquired pre- and post-bleaching. Whole cells were bleached for YFP with the 514-nm argon laser line (80% intensity, 20 iterations, pixel dwell 50.4 µs). The FRET efficiency was calculated from the increase of the donor intensity (CFP) after acceptor bleaching using the FRET module of ZEN 2009 software (Carl Zeiss). FRET efficiency images were generated with a MATLAB script (developed by Dr Felix Neugart, University Stuttgart, Germany) that allows background suppression and visualization of the FRET efficiency at the same time by using a two-dimensional look-up table (total fluorescence intensity coded by pixel brightness, FRET efficiency coded by color). To determine the Golgi-specific increase in RhoA activity, the mean FRET efficiency of the Golgi region was normalized to the mean FRET efficiency of the whole cell. Alexa-Fluor®-633-labeled giantin was excited with the 633-nm helium-neon laser line and its emission was detected from 621–735 nm.

Tfn recycling and surface labeling

For Tfn recycling, cells were starved in serum-free medium prior to incubation with 10 µg/ml Alexa-Fluor®-555-labeled Tfn (Invitrogen) for 1 h. Cells were then rinsed for 45 s with acidic buffer (0.5% acetic acid, 0.5 M sodium chloride, pH 3.0) to remove surface-bound Tfn, followed by washes with PBS and medium containing 10% FCS. During the chase phase, cells were incubated in medium containing 10% FCS for the indicated times. Next, cells were washed with ice-cold PBS and trypsinized for 3 min at 37°C. Finally, cells were washed with ice-cold FACS buffer (PBS+2% FCS+0.1% sodium azide] and analyzed with the EPICS FC500 flow cytometer (Beckman Coulter; Krefeld, Germany). Tfn–555 intensity was measured in the FL-2 channel; unlabeled cells were used for gating. Post-acquisition data analysis was performed using FlowJo software (Tree Star; Ashland, OR). To measure surface-bound Tfn, cells were harvested by trypsinization and washed once with ice-cold FACS buffer. After pre-chilling on ice for 10 min, cells were incubated with 10 µg/ml Alexa-Fluor®-555-labeled Tfn for 45 min. Cells were then washed with ice-cold FACS buffer and processed for flow cytometry as described above.

Tfn uptake assay

Microscopic analysis of Tfn uptake was performed as described previously (Hattula et al., 2006). Briefly, cells were washed with serum-free medium and starved for 1 h. Cells were then incubated with 10 µg/ml Alexa-Fluor®-555-labeled Tfn for 1 h. To remove surface-bound Tfn, cells were rinsed for 45 s with acidic buffer (0.5% acetic acid, 0.5 M sodium chloride, pH 3.0), washed three times with PBS, fixed and processed for immunofluorescence staining.

EGFR trafficking and signaling assays

To analyze EGFR endocytosis, cells were incubated for the indicated times with 200 ng/ml Alexa-Fluor®-555-labeled EGF (Invitrogen), washed with PBS, fixed and processed for immunofluorescence staining. For EGFR signaling experiments, cells were starved overnight in medium supplemented with 0.5% FCS. Cells were then stimulated with either 10 ng/ml EGF (HeLa) or 50 ng/ml EGF (MCF7) for the indicated times. Next, cells were lysed and processed for western blotting.

Acknowledgements

We thank Prof. Dr. Klaus Pfizenmaier (University of Stuttgart, Germany) for critically reviewing the manuscript. We gratefully acknowledge Dr. Felix Neugart (University of Stuttgart, Germany) for developing the MATLAB script. We thank Drs. Lucas Pelkman, Hesso Farhan and Cornelius Knabbe for providing plasmids and cells.

Competing interests

The authors declare no competing or financial interests.

Author contributions

A.C.B., J.H. and S.A.E. performed the experiments and analyzed data; S.S. assisted with cloning. A.H. participated in the experimental design and data analysis. M.A.O. conceived the study and wrote the manuscript together with A.C.B.

Funding

This work was funded by the Deutsche Krebshilfe [grant number 109033]. M.A.O. is funded by the Heisenberg program of the Deutsche Forschungsgemeinschaft.

Supplementary material

Supplementary material available online at
http://jcs.biologists.org/lookup/suppl/doi:10.1242/jcs.163857/-/DC1

References

Adamson, P., Paterson, H. F. and Hall, A. (1992). Intracellular localization of the P21rho proteins. *J. Cell Biol.* **119**, 617-627.
Arthur, W. T. and Burridge, K. (2001). RhoA inactivation by p190RhoGAP regulates cell spreading and migration by promoting membrane protrusion and polarity. *Mol. Biol. Cell* **12**, 2711-2720.
Bard, F., Mazelin, L., Péchoux-Longin, C., Malhotra, V. and Jurdic, P. (2003). Src regulates Golgi structure and KDEL receptor-dependent retrograde transport to the endoplasmic reticulum. *J. Biol. Chem.* **278**, 46601-46606.
Bolte, S. and Cordelières, F. P. (2006). A guided tour into subcellular colocalization analysis in light microscopy. *J. Microsc.* **224**, 213-232.
Bos, J. L., Rehmann, H. and Wittinghofer, A. (2007). GEFs and GAPs: critical elements in the control of small G proteins. *Cell* **129**, 865-877.
Camera, P., da Silva, J. S., Griffiths, G., Giuffrida, M. G., Ferrara, L., Schubert, V., Imarisio, S., Silengo, L., Dotti, C. G. and Di Cunto, F. (2003). Citron-N is a neuronal Rho-associated protein involved in Golgi organization through actin cytoskeleton regulation. *Nat. Cell Biol.* **5**, 1071-1078.
Chi, S., Cao, H., Wang, Y. and McNiven, M. A. (2011). Recycling of the epidermal growth factor receptor is mediated by a novel form of the clathrin adaptor protein Eps15. *J. Biol. Chem.* **286**, 35196-35208.
Durkin, M. E., Yuan, B.-Z., Zhou, X., Zimonjic, D. B., Lowy, D. R., Thorgeirsson, S. S. and Popescu, N. C. (2007a). DLC-1:a Rho GTPase-activating protein and tumour suppressor. *J. Cell. Mol. Med.* **11**, 1185-1207.
Durkin, M. E., Ullmannova, V., Guan, M. and Popescu, N. C. (2007b). Deleted in liver cancer 3 (DLC-3), a novel Rho GTPase-activating protein, is downregulated in cancer and inhibits tumor cell growth. *Oncogene* **26**, 4580-4589.
Egea, G., Serra-Peinado, C., Salcedo-Sicilia, L. and Gutiérrez-Martínez, E. (2013). Actin acting at the Golgi. *Histochem. Cell Biol.* **140**, 347-360.
Erlmann, P., Schmid, S., Horenkamp, F. A., Geyer, M., Pomorski, T. G. and Olayioye, M. A. (2009). DLC1 activation requires lipid interaction through a polybasic region preceding the RhoGAP domain. *Mol. Biol. Cell* **20**, 4400-4411.
Fernandez-Borja, M., Janssen, L., Verwoerd, D., Hordijk, P. and Neefjes, J. (2005). RhoB regulates endosome transport by promoting actin assembly on endosomal membranes through Dia1. *J. Cell Sci.* **118**, 2661-2670.
Gampel, A., Parker, P. J. and Mellor, H. (1999). Regulation of epidermal growth factor receptor traffic by the small GTPase rhoB. *Curr. Biol.* **9**, 955-958.
Goud, B., Zahraoui, A., Tavitian, A. and Saraste, J. (1990). Small GTP-binding protein associated with Golgi cisternae. *Nature* **345**, 553-556.
Grant, B. D. and Donaldson, J. G. (2009). Pathways and mechanisms of endocytic recycling. *Nat. Rev. Mol. Cell Biol.* **10**, 597-608.
Harris, K. P. and Tepass, U. (2010). Cdc42 and vesicle trafficking in polarized cells. *Traffic* **11**, 1272-1279.
Hattula, K., Furuhjelm, J., Tikkanen, J., Tanhuanpää, K., Laakkonen, P. and Peränen, J. (2006). Characterization of the Rab8-specific membrane traffic route linked to protrusion formation. *J. Cell Sci.* **119**, 4866-4877.
Heering, J., Erlmann, P. and Olayioye, M. A. (2009). Simultaneous loss of the DLC1 and PTEN tumor suppressors enhances breast cancer cell migration. *Exp. Cell Res.* **315**, 2505-2514.
Ho, T. T. G., Merajver, S. D., Lapière, C. M., Nusgens, B. V. and Deroanne, C. F. (2008). RhoA-GDP regulates RhoB protein stability. Potential involvement of RhoGDIalpha. *J. Biol. Chem.* **283**, 21588-21598.
Holeiter, G., Bischoff, A., Braun, A. C., Huck, B., Erlmann, P., Schmid, S., Herr, R., Brummer, T. and Olayioye, M. A. (2012). The RhoGAP protein Deleted in Liver Cancer 3 (DLC3) is essential for adherens junctions integrity. *Oncogenesis* **1**, e13.
Horgan, C. P., Oleksy, A., Zhdanov, A. V., Lall, P. Y., White, I. J., Khan, A. R., Futter, C. E., McCaffrey, J. G. and McCaffrey, M. W. (2007). Rab11-FIP3 is critical for the structural integrity of the endosomal recycling compartment. *Traffic* **8**, 414-430.
Jaffe, A. B. and Hall, A. (2005). Rho GTPases: biochemistry and biology. *Annu. Rev. Cell Dev. Biol.* **21**, 247-269.
Johnson, J. L., Monfregola, J., Napolitano, G., Kiosses, W. B. and Catz, S. D. (2012). Vesicular trafficking through cortical actin during exocytosis is regulated

by the Rab27a effector JFC1/Slp1 and the RhoA-GTPase-activating protein Gem-interacting protein. *Mol. Biol. Cell* **23**, 1902-1916.
Kawai, K., Kiyota, M., Seike, J., Deki, Y. and Yagisawa, H. (2007). START-GAP3/DLC3 is a GAP for RhoA and Cdc42 and is localized in focal adhesions regulating cell morphology. *Biochem. Biophys. Res. Commun.* **364**, 783-789.
Lamaze, C., Chuang, T. H., Terlecky, L. J., Bokoch, G. M. and Schmid, S. L. (1996). Regulation of receptor-mediated endocytosis by Rho and Rac. *Nature* **382**, 177-179.
Liu, S. and Storrie, B. (2012). Are Rab proteins the link between Golgi organization and membrane trafficking? *Cell. Mol. Life Sci.* **69**, 4093-4106.
Luna, A., Matas, O. B., Martínez-Menárguez, J. A., Mato, E., Durán, J. M., Ballesta, J., Way, M. and Egea, G. (2002). Regulation of protein transport from the Golgi complex to the endoplasmic reticulum by CDC42 and N-WASP. *Mol. Biol. Cell* **13**, 866-879.
Miserey-Lenkei, S., Chalancon, G., Bardin, S., Formstecher, E., Goud, B. and Echard, A. (2010). Rab and actomyosin-dependent fission of transport vesicles at the Golgi complex. *Nat. Cell Biol.* **12**, 645-654.
Müsch, A., Cohen, D., Kreitzer, G. and Rodriguez-Boulan, E. (2001). cdc42 regulates the exit of apical and basolateral proteins from the trans-Golgi network. *EMBO J.* **20**, 2171-2179.
Nalbant, P., Hodgson, L., Kraynov, V., Toutchkine, A. and Hahn, K. M. (2004). Activation of endogenous Cdc42 visualized in living cells. *Science* **305**, 1615-1619.
Naslavsky, N., Rahajeng, J., Sharma, M., Jovic, M. and Caplan, S. (2006). Interactions between EHD proteins and Rab11-FIP2: a role for EHD3 in early endosomal transport. *Mol. Biol. Cell* **17**, 163-177.
Pathak, R., Delorme-Walker, V. D., Howell, M. C., Anselmo, A. N., White, M. A., Bokoch, G. M. and Dermardirossian, C. (2012). The microtubule-associated Rho activating factor GEF-H1 interacts with exocyst complex to regulate vesicle traffic. *Dev. Cell* **23**, 397-411.
Peränen, J. (2011). Rab8 GTPase as a regulator of cell shape. *Cytoskeleton (Hoboken)* **68**, 527-539.
Pertz, O., Hodgson, L., Klemke, R. L. and Hahn, K. M. (2006). Spatiotemporal dynamics of RhoA activity in migrating cells. *Nature* **440**, 1069-1072.
Platta, H. W. and Stenmark, H. (2011). Endocytosis and signaling. *Curr. Opin. Cell Biol.* **23**, 393-403.
Qualmann, B. and Mellor, H. (2003). Regulation of endocytic traffic by Rho GTPases. *Biochem. J.* **371**, 233-241.
Robertson, D., Paterson, H. F., Adamson, P., Hall, A. and Monaghan, P. (1995). Ultrastructural localization of ras-related proteins using epitope-tagged plasmids. *J. Histochem. Cytochem.* **43**, 471-480.
Roland, J. T., Kenworthy, A. K., Peranen, J., Caplan, S. and Goldenring, J. R. (2007). Myosin Vb interacts with Rab8a on a tubular network containing EHD1 and EHD3. *Mol. Biol. Cell* **18**, 2828-2837.
Salvarezza, S. B., Deborde, S., Schreiner, R., Campagne, F., Kessels, M. M., Qualmann, B., Caceres, A., Kreitzer, G. and Rodriguez-Boulan, E. (2009). LIM kinase 1 and cofilin regulate actin filament population required for dynamin-dependent apical carrier fission from the trans-Golgi network. *Mol. Biol. Cell* **20**, 438-451.
Schenck, A., Goto-Silva, L., Collinet, C., Rhinn, M., Giner, A., Habermann, B., Brand, M. and Zerial, M. (2008). The endosomal protein Appl1 mediates Akt substrate specificity and cell survival in vertebrate development. *Cell* **133**, 486-497.
Settleman, J., Albright, C. F., Foster, L. C. and Weinberg, R. A. (1992). Association between GTPase activators for Rho and Ras families. *Nature* **359**, 153-154.
Sirokmány, G., Szidonya, L., Káldi, K., Gáborik, Z., Ligeti, E. and Geiszt, M. (2006). Sec14 homology domain targets p50RhoGAP to endosomes and provides a link between Rab and Rho GTPases. *J. Biol. Chem.* **281**, 6096-6105.
Stenmark, H. (2009). Rab GTPases as coordinators of vesicle traffic. *Nat. Rev. Mol. Cell Biol.* **10**, 513-525.
Symons, M. and Rusk, N. (2003). Control of vesicular trafficking by Rho GTPases. *Curr. Biol.* **13**, R409-R418.
Tomas, A., Futter, C. E. and Eden, E. R. (2014). EGF receptor trafficking: consequences for signaling and cancer. *Trends Cell Biol.* **24**, 26-34.
Ullrich, O., Reinsch, S., Urbé, S., Zerial, M. and Parton, R. G. (1996). Rab11 regulates recycling through the pericentriolar recycling endosome. *J. Cell Biol.* **135**, 913-924.
Vega, F. M., Fruhwirth, G., Ng, T. and Ridley, A. J. (2011). RhoA and RhoC have distinct roles in migration and invasion by acting through different targets. *J. Cell Biol.* **193**, 655-665.
Vigil, D., Cherfils, J., Rossman, K. L. and Der, C. J. (2010). Ras superfamily GEFs and GAPs: validated and tractable targets for cancer therapy? *Nat. Rev. Cancer* **10**, 842-857.
von Blume, J., Duran, J. M., Forlanelli, E., Alleaume, A.-M., Egorov, M., Polishchuk, R., Molina, H. and Malhotra, V. (2009). Actin remodeling by ADF/cofilin is required for cargo sorting at the trans-Golgi network. *J. Cell Biol.* **187**, 1055-1069.
Wakana, Y., van Galen, J., Meissner, F., Scarpa, M., Polishchuk, R. S., Mann, M. and Malhotra, V. (2012). A new class of carriers that transport selective cargo from the trans Golgi network to the cell surface. *EMBO J.* **31**, 3976-3990.
Wildenberg, G. A., Dohn, M. R., Carnahan, R. H., Davis, M. A., Lobdell, N. A., Settleman, J. and Reynolds, A. B. (2006). p120-catenin and p190RhoGAP regulate cell-cell adhesion by coordinating antagonism between Rac and Rho. *Cell* **127**, 1027-1039.
Xue, W., Krasnitz, A., Lucito, R., Sordella, R., Vanaelst, L., Cordon-Cardo, C., Singer, S., Kuehnel, F., Wigler, M., Powers, S. et al. (2008). DLC1 is a chromosome 8p tumor suppressor whose loss promotes hepatocellular carcinoma. *Genes Dev.* **22**, 1439-1444.
Yadav, S. and Linstedt, A. D. (2011). Golgi positioning. *Cold Spring Harb. Perspect. Biol.* **3**, a005322.
Yamamura, R., Nishimura, N., Nakatsuji, H., Arase, S. and Sasaki, T. (2008). The interaction of JRAB/MICAL-L2 with Rab8 and Rab13 coordinates the assembly of tight junctions and adherens junctions. *Mol. Biol. Cell* **19**, 971-983.
Zilberman, Y., Alieva, N. O., Miserey-Lenkei, S., Lichtenstein, A., Kam, Z., Sabanay, H. and Bershadsky, A. (2011). Involvement of the Rho-mDia1 pathway in the regulation of Golgi complex architecture and dynamics. *Mol. Biol. Cell* **22**, 2900-2911.

Supplementary figure legends

Fig. S1: Functional analysis and subcellular localization of DLC3-WT and -K725E in HeLa cells. (A, B) HeLa cells transiently expressing GFP alone, GFP-DLC3-K725E or GFP-DLC3-WT (green) were stained for phalloidin (red) and nuclei were counterstained with DAPI (blue). Representative maximum projections are shown and imaging parameters were identical. (B) Quantification of the mean fluorescence intensity of phalloidin per cell. Data show the mean ± s.e.m. (n=3, N≥25 cells); ns, not significant; **P=0.0021 (one-way ANOVA followed by Tukey´s post-test). (C) HeLa cells were co-transfected overnight with the RhoA WT biosensor pTriEx-RhoA FLARE.sc and empty FLAG vector, FLAG-DLC3-K725E or FLAG-DLC3-WT, and on the next day, cells were stained for FLAG. FRET efficiencies were measured over the whole cell. Results of the cells from two independent experiments are depicted as the mean ± s.e.m. (N≥40 cells); ns, not significant; ***P<0.0001 (one-way ANOVA followed by Tukey´s post-test). (D) HeLa cells transiently expressing GFP-DLC3-K725E (green) were either stained for Rab6 or TGN46 (red). In the case of RhoB, cells were co-transfected with vectors encoding mCherry-DLC3-K725E (depicted in green) and CFP-RhoB (depicted in red). Scale bars: 10 µm.

Fig. S2: Validation of perinuclear vesiculation and RhoA activation using an independent siRNA targeting DLC3. (A–E) HeLa cells were transfected with control (spControl) and DLC3-specific (siDLC3/spDLC3) siRNAs. (A) Three days post siRNA transfection, cells were stained for Rab8 (green) and nuclei were counterstained with DAPI (blue). The number of cells containing Rab8-positive tubules was counted and normalized to the total number of analyzed cells. Data show the mean ± s.e.m. (n=3, N≥100 cells); *P=0.0306 (paired Student´s t-test). Whole cell lysates were analyzed by western blotting with anti-DLC3 and anti-tubulin antibodies. (B) Three days post siRNA transfection, cells were stained for giantin (green) and nuclei were counterstained with DAPI (blue). Golgi fragmentation was calculated for the Golgi markers giantin, GM130 and p230. Values of one representative experiment were normalized to the mean Golgi compaction index of control cells. Data show the mean ± s.e.m. (N≥20 cells); **P<0.01; ***P<0.001 (two-way ANOVA followed by Bonferroni post-test). (A, B) Scale bars: 10 µm. (C, D) Two days post siRNA transfection, cells were transfected with the pTriEx-RhoA WT FLARE.sc biosensor and, on the next day, stained with giantin-specific primary and Alexa Fluor 633-conjugated secondary antibodies. (C) FRET acceptor photobleaching was performed as described in Fig. 4. Scale bars: 5 µm. (D) The mean FRET efficiencies within the

cell and at the Golgi of one representative experiment are plotted as the mean ± s.e.m. (N≥12 cells); upper graph, *P=0.0329, lower graph, *P=0.0325 (unpaired Student´s t-test). (E) Two days post siRNA transfection, cells were transfected with vectors encoding the DLC3 GAP domain fused to DLC3-SAM (SAM-GAP) or DLC3-SAM alone (SAM). Cells were fixed and stained for giantin 24 h later. The Golgi compaction index was calculated for at least three independent experiments. Values were normalized to untransfected control cells. Data show the mean ± s.e.m. (n=3-6, N≥50 cells); ns, not significant; **P<0.01; ***P<0.001 (two-way ANOVA followed by Bonferroni post-test).

Fig. S3: Cytoskeletal changes in cells lacking DLC3. HeLa cells were transfected with control (spControl) and DLC3-specific (spDLC3) siRNAs. Three days post transfection, cells were stained for paxillin (green) and phalloidin (red), nuclei were counterstained with DAPI (blue). Scale bars: 10 µm.

Fig. S4: DLC3 depletion alters EGFR trafficking and prolongs EGFR signaling. (A) HeLa cells were transfected with control (spControl) or DLC3-specific (spDLC3) siRNAs. Three days post siRNA transfection, cells were incubated with EGF-555 (red) for 120 min and either stained for EEA1 or Rab7 (green). Nuclei were counterstained with DAPI (blue). Scale bars: 10 µm. (B) MCF7 cells were transfected with control (spControl) or DLC3-specific (spDLC3) siRNAs. Two days post siRNA transfection, cells were serum-starved overnight and, prior to lysis, stimulated with 50 ng/ml EGF for the indicated times. Whole cell lysates were analyzed by western blotting with anti-pAKT (Thr308; arrow), anti-AKT, anti-pERK (Thr202/Tyr204), anti-ERK and anti-tubulin antibodies. One representative western blot out of two independent experiments is shown.

Fig. S1

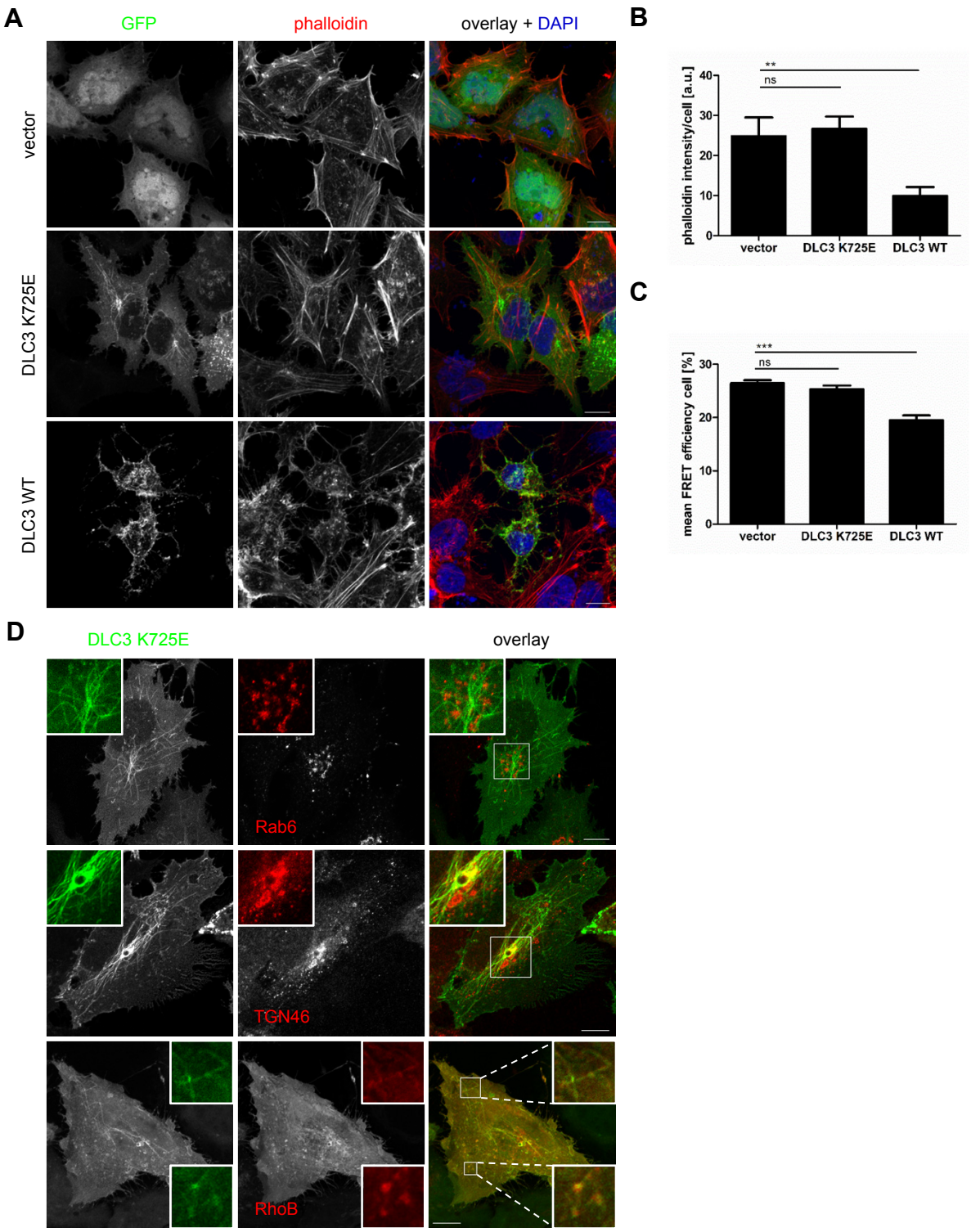
A
GFP
phalloidin
overlay + DAPI
vector
DLC3 K725E
DLC3 WT
B
phalloidin intensity/cell [a.u.]
**
ns
vector
DLC3 K725E
DLC3 WT
C
mean FRET efficiency cell [%]
***
ns
vector
DLC3 K725E
DLC3 WT
D
DLC3 K725E
overlay
Rab6
TGN46
RhoB

Fig. S2

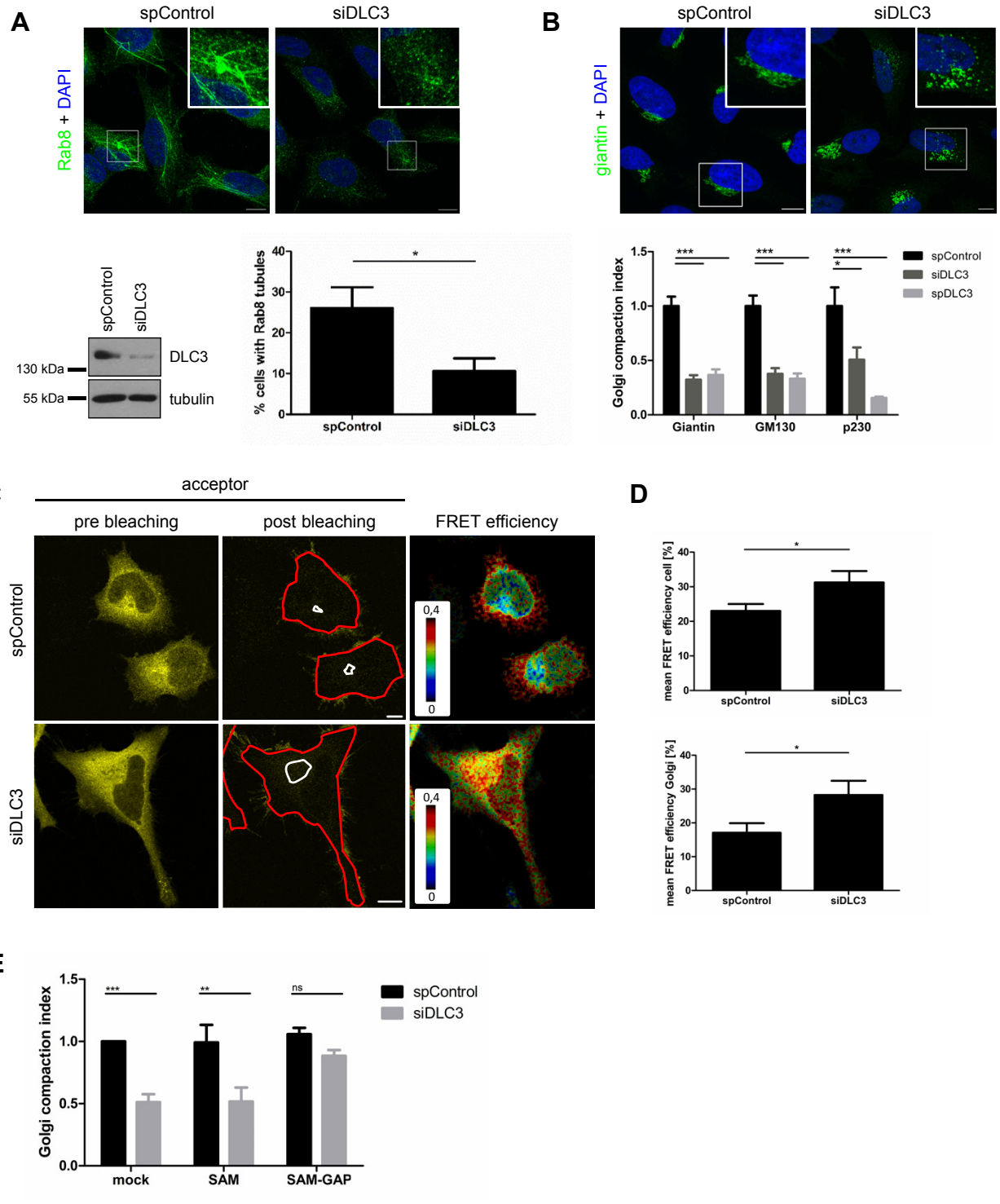
A
spControl
siDLC3
Rab8 + DAPI
spControl
siDLC3
130 kDa
55 kDa
DLC3
tubulin
% cells with Rab8 tubules
spControl
siDLC3
B
spControl
siDLC3
giantin + DAPI
Golgi compaction index
Giantin
GM130
p230
spControl
siDLC3
spDLC3
C
acceptor
pre bleaching
post bleaching
FRET efficiency
spControl
siDLC3
0,4
0
D
mean FRET efficiency cell [%]
spControl
siDLC3
mean FRET efficiency Golgi [%]
spControl
siDLC3
E
Golgi compaction index
mock
SAM
SAM-GAP
spControl
siDLC3

Fig. S3

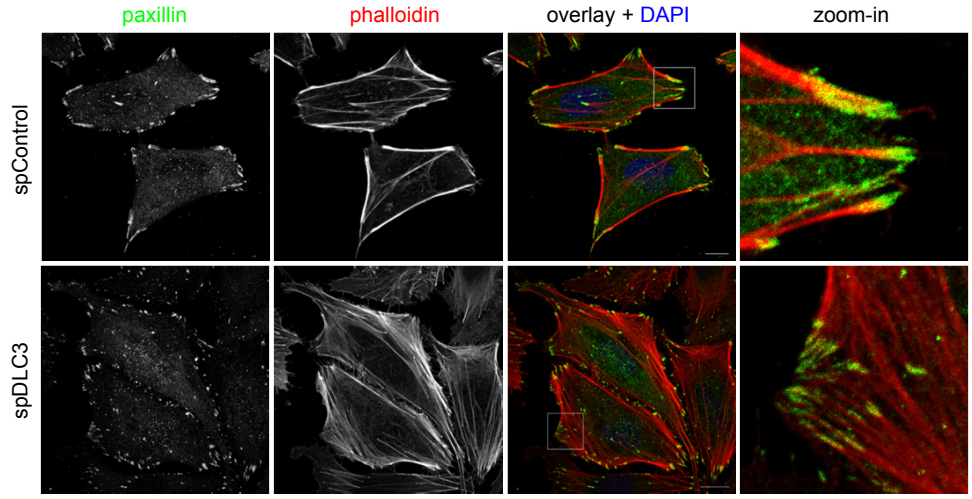
paxillin
phalloidin
overlay + DAPI
zoom-in
spControl
spDLC3

Fig. S4

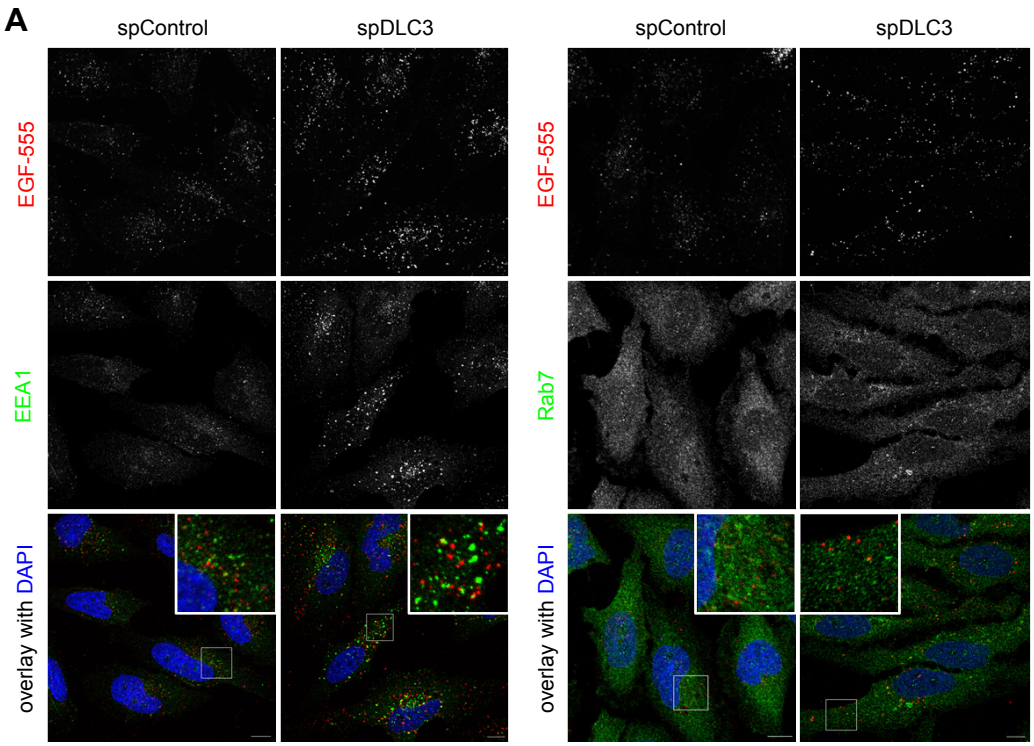
A
spControl
spDLC3
spControl
spDLC3
EGF-555
EEA1
overlay with DAPI
EGF-555
Rab7
overlay with DAPI

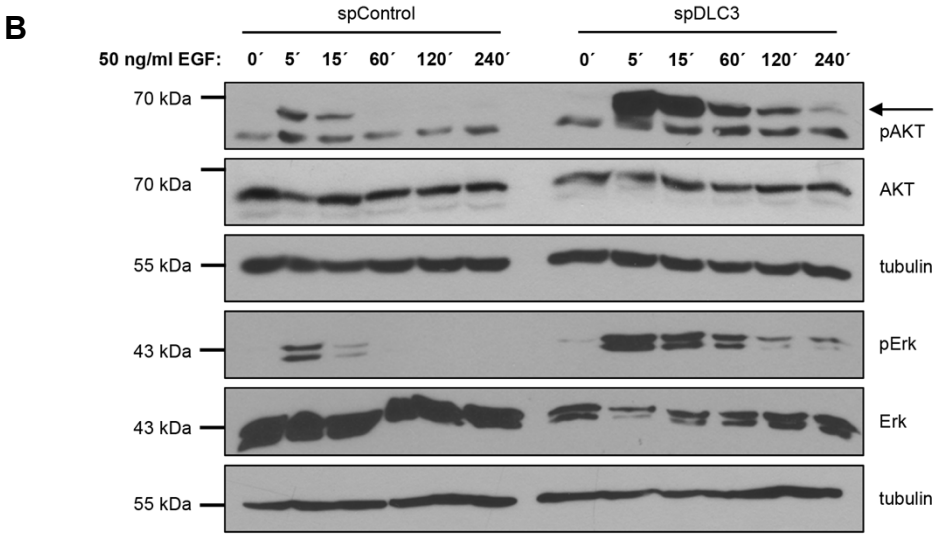
B
spControl
spDLC3
50 ng/ml EGF:
0´ 5´ 15´ 60´ 120´ 240´
0´ 5´ 15´ 60´ 120´ 240´
70 kDa
pAKT
70 kDa
AKT
55 kDa
tubulin
43 kDa
pErk
43 kDa
Erk
55 kDa
tubulin